2.3 Electrical properties of the earth's interior
See p. 370
2.4 Composition of the earth's interior
2.5 Tides of the earth
3 Gravity field and figure of the earth
See Subvolume V/2a

4 Magnetic field of the earth

4.1 Sources of the geomagnetic field

4.1.1 External part of the earth's magnetic field

4.1.1.0 Components of the field, units

List of symbols and abbreviations

Ap	planetary index of daily geomagnetic activity (linear scale)
a_n^m, b_n^m	spherical harmonic coefficients for Z
$\boldsymbol{B}$	flux density (=induction) vector of the earth's magnetic field (geomagnetic variations), in [nT] ($1\,\mathrm{nT} \triangleq 10^{-5}$ G)
C_0	complex-valued inductive scale length ("penetration depth") for zero wavenumber, in [km]
Cp	planetary index of daily geomagnetic activity (quasi-logarithmic scale)
c_n^m, γ_n^m	spherical harmonic coefficients for internal (c) and external (γ) parts of potential V ($\cos m\lambda$-terms), in [nT]
D	angle of magnetic declination, in [deg]; magnetic east component of geomagnetic variations, i.e. variations normal to the local magnetic meridian, in [nT]
$\delta(\omega, z)$	complex-valued attenuation factor
g_n^m, h_n^m	spherical harmonic coefficients for X, Y, in [nT]
H	horizontal magnetic intensity (=tangential component of $\boldsymbol{B}$ at the earth's surface); horizontal geomagnetic variations parallel to local magnetic north, in [nT]
j	sheet current density, in [A/m]
K, Kp	three-hourly local and planetary index of geomagnetic activity (quasi-logarithmic scale), respectively
k	wavenumber
μ_0	magnetic permeability of the vacuum $\mu_0 = 4\pi \cdot 10^{-7}$ Vs/Am
$v = \tau - T$	phase of the moon
$p(\omega)$	skin depth
pc, pi, pg	regular, irregular, and giant geomagnetic pulsations, respectively
$P_n^m(\cos\theta)$	associated spherical harmonic function, quasi-normalized after A. Schmidt; θ: angle of colatitude
r, θ, λ	geocentric spherical coordinates
R	sunspot number
R_E	(equivolumetric) earth's radius: $R_E = 6371$ km (MAGSAT: $R_E = 6371.2$ km)
ϱ	electrical resistivity, in [Ωm]
s_n^m, σ_n^m	spherical harmonic coefficients for internal (s) and external (σ) parts of potential V ($\sin m\lambda$-terms), in [nT]
σ	electrical conductivity, in [$\Omega^{-1}\,m^{-1}$]
σ_n^2	degree variance, in [nT^2]
T	solar mean local time, in angular measure ($1\,h \triangleq 15°$)
t	universal (=Greenwich) time
τ	lunar mean local time, in angular measure ($1\,h \triangleq 15°$); conductance of sediment layers or oceans, in [S]
Φ	geomagnetic latitude
V	magnetic potential ($\boldsymbol{B} = -\mathrm{grad}\ V$), in [Vs/m]
x, y, z	rectangular coordinates (geographic north, east, down, respectively)
X, Y, Z	rectangular components of $\boldsymbol{B}$ (geographic north, east, down, respectively), in [nT]
ω	angular frequency, in [s^{-1}]

Abbreviations

DP	disturbed polar geomagnetic variations: DP1, DP2
Dst, DS	smoothed storm-time geomagnetic variations
EEJ	equatorial electrojet
ELF	extra low frequency emission (3···3000 Hz)
ERC	equatorial ring current in the radiation belt of the magnetosphere
L	lunar daily geomagnetic variations
PEJ	polar electrojet
S	solar daily geomagnetic variations
Sq, S_q^P, S_D	S on quiet days in middle and low latitudes, in polar latitudes, on disturbed days, respectively
sfe	geomagnetic solar flare effect
ssc	sudden storm commencement
VLF	very low frequency emission (3···30 kHz)

By convention field observations in geomagnetism are interpreted as measurements of the free-space flux density $\boldsymbol{B}=\mu_0\boldsymbol{H}$ of the earth's magnetic field; $\mu_0=4\pi\cdot10^{-7}$ Vs/Am for S.I. units and $\boldsymbol{H}$ denotes the magnetic field strength. The following symbols are conventional for the components of $\boldsymbol{B}$: Z for the vertical component with regard to the earth's surface (down positive), H for the horizontal intensity, X and Y for the geographic north and east components of H, respectively, F for the total intensity $|\boldsymbol{B}|$.

The ratio $Z/H=\tan I$ defines the angle of inclination, the direction of H as shown by the compass needle defines magnetic north and thereby the direction of the local magnetic meridian. The angle between magnetic and geographic north is the angle of declination D, on nautical charts also called "magnetic variation". D is positive when magnetic north is eastward from geographic north, i.e. $\mathrm{tg}\,D=Y/X$. See eqs. (1) and (4) in subsect. 4.2.3.1.2 for relations which connect these elements of the geomagnetic field and their derivation from a magnetic potential.

In studies of geomagnetic variations the total field $\boldsymbol{B}$ is separated into an undisturbed part and a disturbance ΔB. The components of ΔB are observed usually in a references frame defined by the local magnetic meridian of the undisturbed field; ΔH, ΔD, ΔZ are then the magnetic north, the magnetic east, and the vertical component of ΔB, respectively. Except for polar regions, ΔD is small against H and the disturbance in declination is approximately $\Delta D/H$. Since this is the observed quantity at many observatories, it is also denoted by ΔD. For global investigations ΔB is referred to geographic coordinates using the declination of the undisturbed field for the rotation of coordinates, which gives ΔX, ΔY, ΔZ as geographic north, geographic east, and vertical component of ΔB, respectively. Since subsect. 4.1.1 deals exclusively with the disturbance field, the letter Δ is omitted in the following.

The conventional unit for $\boldsymbol{B}$ in geomagnetism is 1 nanotesla, $1\,\mathrm{nT}=10^{-9}\,\mathrm{Vs/m^2}$. It is identical with the formerly used unit 1 gamma, $1\,\gamma=10^{-5}$ Gauss (G or Γ). Note that for a long time this cgs-unit has been also the unit for the magnetization of rocks. Then $1\,\gamma$ corresponds to 0.01 A/m in S.I. units.

To visualize fields with flux densities of 1 nT consider the following examples: An infinitely long wire carrying a current of 1 A produces 1 nT at a distance of 200 m. The same flux density has the field which a dipole of moment $1\,\mathrm{Am^2}$ generates at $\sqrt[3]{100}=4.64$ m distance in its equatorial plane. The field above a uniform sheet current with the density 1 A/km has a flux density of 0.628 nT. The same flux density exists in the center of a circular current loop of 1 m radius with 1 mA.

4.1.1.1 Planetary field, interplanetary field, and geomagnetic variations

The earth like some but not all planets in the solar system has a planetary field of internal origin. At the earth's surface it has dipole character with a flux density of about 60000 nT near the poles and 30000 nT at the equator. At a given site slow field changes are observed on a secular time scale, a typical rate of change is 10 nT/a.

The planetary field is bounded outside the earth by interaction with the solar wind and confined to a region known as the magnetosphere (Fig. 1). Beyond this region an interplanetary field exists of about 5 nT which is of solar origin.

Within the magnetosphere shifting and intermittent electric currents are generated by solar radiation and by interaction with particle streams from the sun. They produce fluctuating magnetic fields which are observed as external part of geomagnetic variations at the earth's surface. The amplitude of these variations rarely exceeds 100 nT in low and mid-latitudes. Near to the dip equator of zero inclination and particularly in polar regions they are enhanced and may exceed in the auroral zones 1000 nT. Slow and fast variations occur. Typical periods lie between 1 day and 1 second (Figs. 2, 13).

Geomagnetic variations are predominantly, but not exclusively, of external origin. The internal part of geomagnetic variations is the magnetic field of electric currents which are induced by the external part in conducting layers of the earth, including the extremely well conducting oceans and some geological formations on continents.

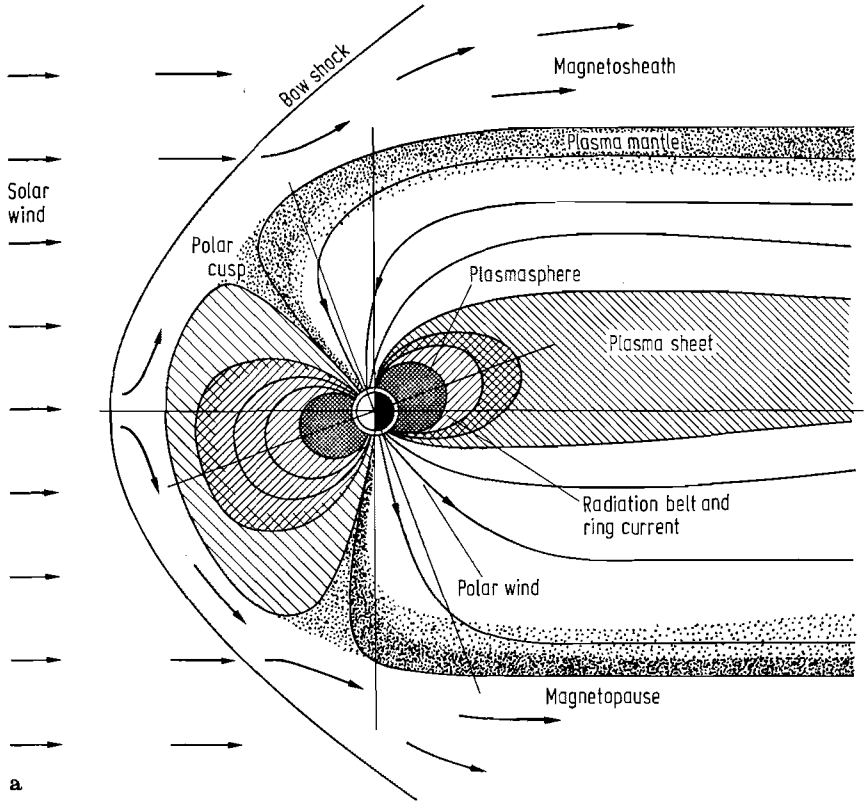

Fig. 1a, b. Cross sections through the undisturbed magnetosphere during solar quiet times. The direction to the sun is indicated, the scale is the earth's radius $R_E = 6371$ km.
a) Model cross section in the noon-midnight meridional plane of the geomagnetic dipole. Lines with arrow marks inside the magnetosphere are field lines of the earth's dipole field which by interaction with the solar wind (cf. text) is compressed on the day-side and drawn into a geomagnetic tail on the night-side. The earth's magnetic field ends at the magnetopause as indicated. A possibly turbulent transition region separates as magnetosheath the magnetosphere from the interplanetary space, bounded by the bow shock of a shock wave propagating within the solar wind. Regions of increased charged particle density within the magnetosphere are indicated by various signatures (plasma mantle, plasmasphere, plasma sheet), including the radiation belt of gyrating trapped particles, the source region of Dst variations. From [Ros75].

For Fig. 1b, see next page.

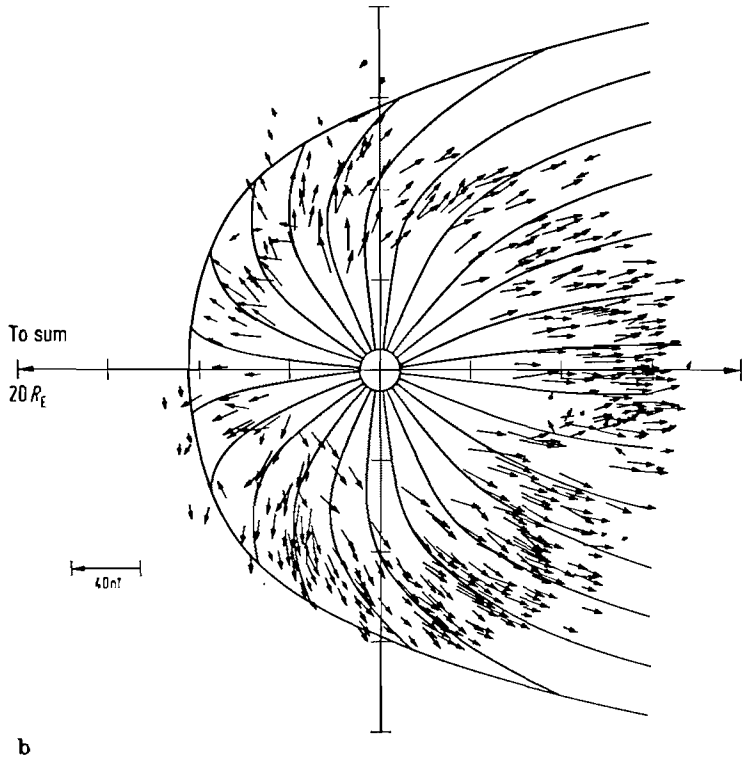

b

Fig. 1b. Cross section in the equatorial plane of the geomagnetic dipole. The field vectors are from satellite observations of the magnetospheric field, projected onto this plane. Solid lines indicate the resulting field line pattern. From [Far68].

►

Fig. 2. Two 24-hour records of the earth's magnetic field, observed at a mid-latitude site. Vertical bars mark full hours in universal time UT; add 54 minutes for local time. Time-varying distances of the traces from a fixed reference line B demonstrate geomagnetic variations in declination D, vertical downward intensity Z, and horizontal intensity H. See Table 6 in subsect. 4.2.3 for absolute values. An angular change of declination by one minute of arc corresponds here to an east component D of the disturbance field of 5.6 nT.

Upper magnetogram: Solar daily variations Sq on a quiet day with $Kp \leqq 2-$ (cf. 4.1.1.7 and Fig. 20). A solar flare effects sfe is recorded shortly after 14 h UT (cf. text). Upward D departures from the midnight level in the morning (the compass needle swings east by 8') indicate overhead Sq currents toward the equator, downward departures of similar size in the early afternoon the closure of the Sq current loop by northward currents (Fig. 5). The nearly overhead passage of the center of the current loop causes the downward departure in Z by 40 nT near noon.

Lower magnetogram: Regular Sq variations are terminated abruptly by a sudden storm commencement ssc at 19^h12^{min} UT, whichs marks the onset of irregular DP variations in the course of a weak magnetic storm with $Kp \leqq 6o$.

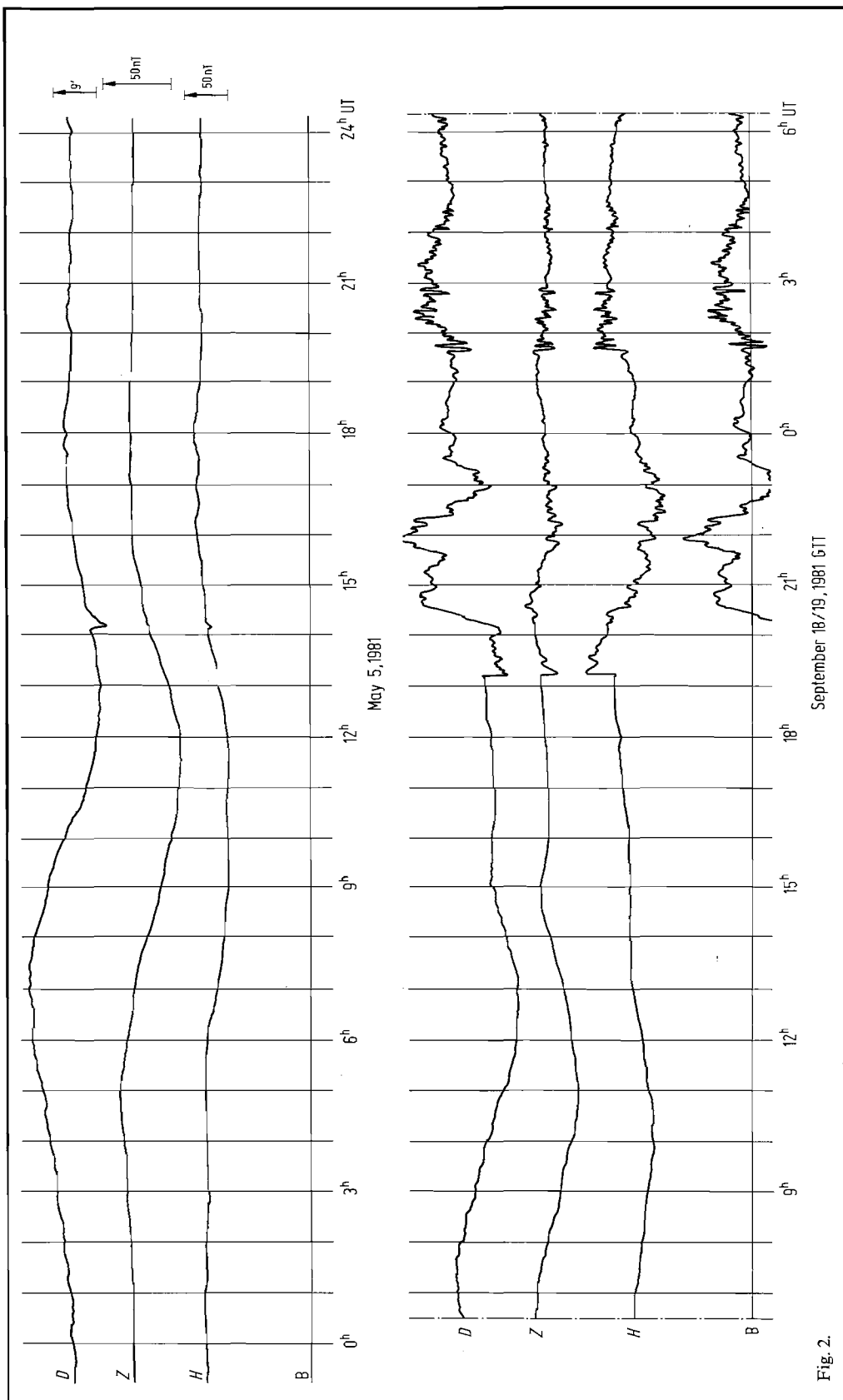
9'
50nT
50nT
24h UT
21h
18h
15h
12h
9h
6h
3h
0h
May 5, 1981
D
Z
H
B
6h UT
3h
0h
21h
18h
15h
12h
9h
September 18/19, 1981 GTT
D
Z
H
B

Fig. 2.

4.1.1.2 Classification of geomagnetic variations

Table 1. Symbol, period, and amplitude of geomagnetic variations.
τ: Fundamental period for regular variations, period range for irregular variations.
A: Peak-to-peak amplitude or maximum departure from undisturbed level.
If a pronounced dependence on latitude exists, different values are quoted for auroral zone (a), mid-latitudes (m), low latitudes (l), and the dip equator region on the day-side (dd).

Type	Symbol	τ	A nT	Sample record in Fig.	Source
Solar cycle variations		11 years	20	16	ERC modulation by sunspot cycle
Annual variations		1 year	5		Ionospheric sources
Semi-annual variations		6 months	5		ERC modulation within the earth's orbit around the sun
Smoothed storm-time variations					Enhanced ERC after magnetic storms
storm-time-dependent part	Dst	2···27 d	100	14, 15	
disturbance local time inequality	DS	12···24 h	100	15	
Solar daily variations	S	1 d			
on quiet days	Sq		30···60 (m, l) 60···120 (dd)	2, 6, 9	Ionospheric current loops on day-side sectors of both hemispheres (Fig. 5)
enhancement on disturbed days	S_D	1 d	10···20		
Lunar daily variations	L	1 d	1···3	11	Dual ionospheric current loops on both hemispheres (Fig. 10)
Polar magnetic storms and short-lived substorms	DP	10 min···2 h			
centre of disturbance in the night-time auroral zone	DP1		1000 (a) 100 (m, l)	13a	Polar electrojet PEJ in the ionosphere with connecting field-aligned currents to plasma regions of the magneto-sphere (Figs. 1a, 12)
with correlated irregular variations in low latitudes	DP2		100 (a) 10 (m, l) 100 (dd)		
Special effects in connection to polar magnetic storms					
bays = substorms as observed in mid-latitudes	b	30 min···2 h	20···100 (a, m) 5···25 (l)	13b	see DP1
Sudden storm commencement	ssc	2···5 min	10···100	2	Impact of intense solar particle stream on magnetopause
Solar flare effect	sfe	10···20 min	10	2	Short-lived enhancement of Sq currents in the ionosphere

continued

Table 1 (continued)

Type	Symbol	τ	A nT	Sample record in Fig.	Source
Pulsations (=ultralow frequency emissions)	P ULF	0.2···600 s		18	Standing and propagating hydromagnetic waves in the magnetosphere
regular continuous pulsations	pc	150···600 s (pc5)	100 (a) 10 (m)		
		45···150 s (pc4)	2		
		5···45 s (pc2, 3)	0.5		
		0.2···5 s (pc1)	0.1		
irregular transient pulsations	pi	1···100 s	1		
Schumann resonance oscillations		1/7.8 s	<0.1		Cavity resonance earth-ionosphere for electromagnetic waves
Extra low frequency emissions, including atmospherics	ELF	10^{-3}···0.2 s	<0.1		Propagating electromagnetic waves in the earth-ionosphere wave guide (ELF) and propagating hydromagnetic waves in the magnetosphere (VLF and ELF)
Very low frequency emissions, including whistlers	VLF	10^{-5}···10^{-3} s			

From their appearance in the magnetograms regular and irregular variations are distinguished (Fig. 2). The most important regular variations are those which occur daily as S variations (S=solar) and L variations (L=lunar), respectively. Both have one solar day as fundamental period. For L the phase of its harmonic constituents varies in time with the changing position of the moon. See the phase law of L variations, eq. (8).

S and L variations are denoted as geomagnetic tides because tidal motions in the high atmosphere are involved. Equally important are solar heating of the atmosphere (for S only) and the ionisation of atmospheric layers on the day-lit side of the earth. In the long time trend of the earth's magnetic field over years the modulation of geomagnetic activity with the sunspot cycle produces regular solar cycle variations with a fundamental period of 11 years.

While S and L regular variations are connected to solar wave radiation, irregular variations arise almost exclusively from solar particle radiation. This solar wind comes from three sources:

(i) Ejections from active regions on the sun, connected to solar flares.

(ii) High speed streams of solar plasma, leaving the sun from coronal holes and providing a continuous activity. Their overall strength varies with the sunspot cycle.

(iii) A steady background stream of solar particles into space due to the high temperature of the solar corona.

When, during active times, the particle stream from the sun is intensified, the magnetosphere is compressed and particles cross the boundary between interplanetary and planetary field. Following field lines of the planetary field, particles can penetrate deeply into the atmosphere near the poles. This is a two-stage process involving (i) particle injection from the plasma sheet of the geomagnetic tail, (ii) secondary acceleration of these particles in the high atmosphere resulting in shifting and fluctuating current systems with associated magnetic fields. They are observed as polar magnetic storms DP (D=disturbed) at the ground, usually accompanied by auroral lights in high latitudes.

Storms are followed by a recovery phase after magnetic quietness has returned when, for several days, ring currents of trapped particles encircle the earth. The slowly decaying magnetic field of this current extends magnetic storms as Dst variations (st=storm) into quiet days. Isolated disturbances which last only for a few hours and which are not followed by a Dst recovery phase are denoted as polar substorms, in mid-latitudes as bays.

It appears that plasma in the magnetosphere can be excited to vibrate in resonance along field lines. The eigenperiod lies between 1 and about 5 minutes. These plasma vibrations produce fluctuating magnetic fields of the same period, which are observed as pulsations of the geomagnetic field on the ground. Various processes in the atmosphere and magnetosphere produce even faster oscillating fields. The VLF electromagnetic wave emissions and whistlers extend the spectrum of geomagnetic variations up to 20 kHz in frequency.

The classical reference to geomagnetic variations is [cha40], modern references are [aka72, aka77, mat67, nis78, par83].

4.1.1.3 Separation of external and internal parts of geomagnetic variations

Quasi-stationary magnetic fields which are observed at the earth's surface can be separated into parts from sources within and outside the earth. No assumptions are needed about cause or location of their sources. By excluding, in quasi-stationary approximation, vertical electric currents above the ground, the magnetic surface field is a potential field. Its flux density $\boldsymbol{B}$ can be derived from the gradient of a scalar potential V: $\boldsymbol{B} = -\text{grad}\, V$, with $\nabla^2 V = 0$.

Let, for simplicity, the earth's surface be flat and form the (x, y)-plane of Cartesian coordinates with z downward positive. The field is sinusoidal in x for planes parallel to the surface, k a real and positive wavenumber for a wavelength $2\pi/k$. Then the z-dependence of the potential must be expotential to satisfy the Laplace equation: $V(x, z) = V_0 \cos kx \cdot \exp(\pm kz)$. The sign of the exponent depends on the position of the sources with regard to the plane of observation. Fields with sources above $z=0$ disappear with $\exp(-kz)$ for $z \to +\infty$ and those with sources below $z=0$ with $\exp(+kz)$ for $z \to -\infty$. The superposition of both fields gives in the space between sources

$$V(x, z) = \{\gamma e^{-kz} + c e^{+kz}\} \cos kx; \tag{1}$$

γ and c denote the potential Fourier coefficients for the field of external and internal origin, respectively. The components of the field in the $z=0$ plane are

$$\begin{aligned} B_x &= -\partial V/\partial x = k\{\gamma + c\} \sin kx \\ B_z &= -\partial V/\partial z = k\{\gamma - c\} \cos kx. \end{aligned} \tag{2}$$

Since from B_x (as function of x) the sum of external and internal coefficients is known, and from B_z their difference, the observed surface field is separable. Note that a vanishing vertical field B_z indicates equal contributions of external and internal sources to the horizontal field B_x.

By adding a sinusoidal dependence on y, three-dimensional fields can be separated in the same way. For applications to fields on a spherical earth's surface, the trigonometric functions have to be replaced by spherical harmonics (cf. subsects. 4.1.3 and 4.2.3.1.2).

See Table 2 for the separation of daily variations, and [Har63] and [Pri63] for alternative separation methods which do not require representations by plane or spherical harmonic functions.

4.1.1.4 Equivalent currents

Equivalent currents as in Figs. 5 and 10 are hypothetical sheet currents in thin spherical shells above or below the earth's surface. Their current density $\boldsymbol{j}$ (unit: A/m) is such that either the external or the internal part of a given magnetic potential field is exactly reproduced. See subsect. 4.1.3.4 for the calculation of $\boldsymbol{j}$ from a given set of spherical harmonic coefficients.

The equivalent current systems for the external part of DP variations in Fig. 12 are not based on a spherical harmonic analysis because their surface fields have too many local details in high latitudes. Instead it is assumed that external and internal currents contribute to the horizontal components in comparable portions. The equivalent currents are such that they reproduce a certain fraction (1/2, 2/3) of the observed horizontal components at a given instant of time. The vertical component is disregarded. See subsect. 4.2.2.4 for details.

Because the planetary field and geomagnetic variations are generated by electric currents, equivalent currents provide an image of their true sources provided the chosen radius of the shell which carries them approximates the correct position of source currents. The concept of equivalent currents has a principal deficiency, however, because it is derived for magnetic potential fields and thus excludes poloidal source currents with radial components. Such currents exist in the source region of geomagnetic variations and, most likely, also in the source region of the planetary field, the earth's outer core. Poloidal currents have toroidal (=tangential) magnetic fields which, in quasi-stationary approximation, do not exist in non-conducting spaces. These sources are unobservable at the earth's surface, leaving a principal ambiguity in the interpretation of magnetic surface observations.

4.1.1.5 Magnetic fields of external origin within the earth

Two effects reduce geomagnetic fields of external origin inside the earth, (i) the increasing distance from the source (geometric effect), and (ii) the shielding by electromagnetically induced currents (skin effect). The geometric effect is a frequency-independent reduction of the field amplitude, the skin effect a frequency-dependent reduction of amplitude and rotation of phase ϕ, the time factor being $\exp i(\omega t+\phi)$. The skin effect dominates if the spatial scale length of the field exceeds the penetration depth C_0 at the considered angular frequency ω, and vice versa.

A typical scale length is the reciprocal wavenumber k^{-1} of a sinusoidal field, a minimum value the height of the sources above the ground. Typical values of $|C_0|$ are 10···20 km for pulsations (period: 1 minute), 100··· 200 km for D variations (period: 1 hour), and 400···600 km for S variations (period: 1 day). See subsect. 4.2.2.2.3 for the definition of C_0. The quoted values refer to observations on continents. They are smaller in oceans.

Because the minimum height of external sources is about 100 km (ionospheric E layer), the geometric effect will be important only for slow variations, e.g. bay variations in auroral zones, and S variations everywhere. Fig. 3 shows the complex-valued attenuation factor $\delta(\omega, z)=\tilde{B}_x(\omega, z)/\tilde{B}_x(\omega, 0)$ in polar diagrams with the depth z as parameter of the attenuation spiral; $\tilde{B}_x(\omega, z)$ denotes the complex Fourier amplitude of the horizontal component. The polar distance to any point on the spiral gives the attenuated relative amplitude $|\delta|$ at the respective depth, the angle against the polar axis the phase relative to the phase of the surface field. The following formulas are for simple estimates of the attenuation factor when the skin effect dominates:

1. Uniform lithosphere of resistivity ϱ: With the definition of the skin depth

$$p(\omega)=\sqrt{\frac{2\varrho}{\omega\mu_0}}, \tag{3}$$

$$\delta(\omega, z)=e^{-z/C(\omega)}, \quad \text{with} \quad C(\omega)=p(\omega)/(1+i). \tag{4a}$$

For a typical value of $\varrho=50\,\Omega$m, the skin depth is 28 km for pulsations (period: 1 minute). In this depth their amplitude is reduced to $e^{-1}\approx 1/3$ and their phase rotated by 1 rad $\triangleq 57.3°$.

2. Non-conducting crystalline basement of thickness h above uniform lower lithosphere of resistivity ϱ:

$$\delta(\omega, z)=\begin{cases}1, & z\leqq h\\ e^{-(z-h)/C(\omega)}, & z>h.\end{cases} \tag{4b}$$

3. Sediments or oceans of conductance τ (=mean conductivity $\bar{\sigma}$ times thickness d, $d^2\ll 2/\bar{\sigma}\omega\mu_0$) above a uniform lithosphere of resistivity ϱ:

$$\delta(\omega, z)=\begin{cases}1-\dfrac{z}{d}\,\dfrac{i\omega\mu_0\tau\, C(\omega)}{1+i\omega\mu_0\tau\, C(\omega)}, & z\leqq d\\ \delta(\omega, d)\cdot e^{-(z-d)/C(\omega)}, & z>d.\end{cases} \tag{4c}$$

For a typical conductance of oceans, $\tau=16000$ S (4000 m of seawater with $\varrho=0.25\,\Omega$m) and a lithosphere of $\varrho=50\,\Omega$m:

$$\delta(\omega, d)=\begin{cases}0.13-0.10\,i & \text{for bays (period: 1 hour)}\\ 0.48-0.21\,i & \text{for Sq (period: 1 day).}\end{cases}$$

Hence, fast variations with periods shorter than 1 hour are shielded from the lithosphere by deep oceans, while daily variations penetrate through them with about half their amplitude. Seafloor observations confirm these conclusions (Fig. 4). See [Bab80] for observations in deep mines below sediments.

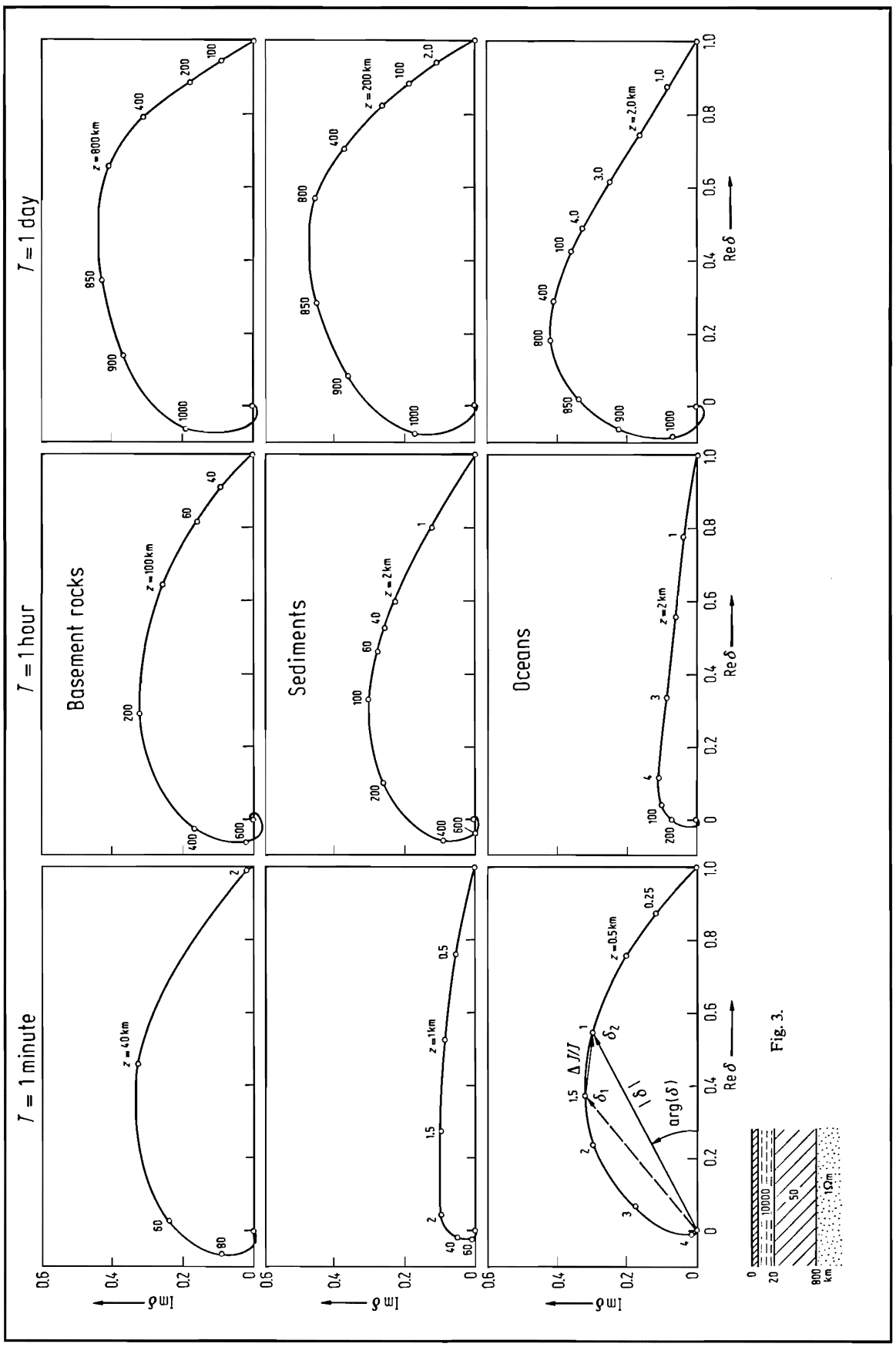
T = 1 minute
T = 1 hour
T = 1 day
Basement rocks
Sediments
Oceans
z = 40 km
z = 100 km
z = 800 km
z = 1 km
z = 2 km
z = 200 km
z = 0.5 km
z = 2.0 km
Re δ
Im δ
Δ H/H
δ1
δ2
|δ|
arg(δ)
10000 Ωm
50 Ωm
1 Ωm
0
20
800 km

Fig. 3.

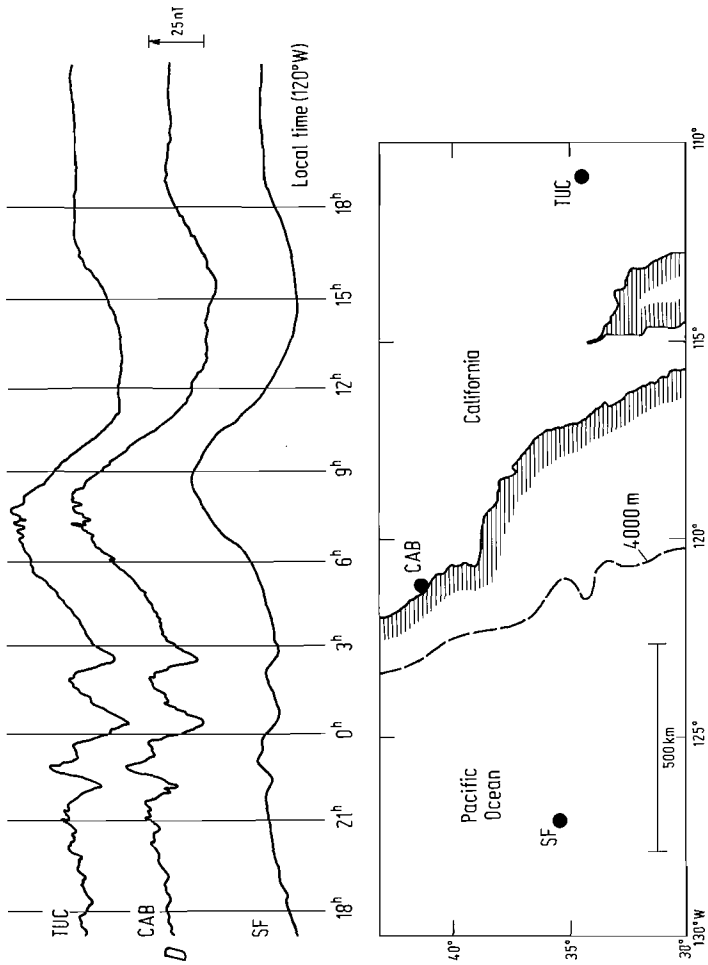

Fig. 4. Skin effect of various types of geomagnetic variations, demonstrated by simultaneous recordings on land (CAB: Cambria, TUC: Tucson), and at the seafloor (SF) in more than 4000 m depth. The strong attenuation of horizontal variations in D (magnetic east component) by induction in the ocean is evident from the small amplitude of night-time DP variations as recorded at the seafloor. Early morning pulsations are wiped out here completely. The less prominent amplitude reduction of seafloor daily variations indicates the diminishing skin effect with increasing period. Differences in longitude are responsible for the apparent phase shift of daily variations between sites. Adopted from [Fi67].

▲ Fig. 3. Electromagnetic skin effect of geomagnetic variations of period T in various earth models of electrical resistivity consisting of a highly resistive crust ($\varrho = 10000\ \Omega$m), a moderately conducting mantle ($\varrho = 50\ \Omega$m) above 800 km depth, and a well conducting mantle ($\varrho = 1\ \Omega$m) below. The skin effect is shown for three different periods and a surface cover of, respectively, basement rocks (2 km, 1000 Ωm), sediments (2 km, 1 Ωm), and oceans (4 km, 0.25 Ωm). Polar diagrams (complex δ-planes) represent the complex valued Fourier amplitude $\delta(\omega, z)$ of horizontal variations at depth z, normalized with respect to their surface amplitude (cf. text). The numbers along the skin effect spirals give the depth in [km]. The contribution $\Delta J/J$ of currents ΔJ induced in the depth range $z_2 \ldots z_1$ to the total depth-integrated current J (cf. eq. (20) in subsect. 4.2.2.3.5) is determined in phase and amplitude by the complex number $\delta_2 - \delta_1$, see $T = 1$ min and ocean surface cover. In the absence of conducting surface layers the skin effect takes place deep within crust and mantle for slow pulsations, polar substorms, and daily variations. Sediments and oceans shift the induction toward the uppermost layers. Note the resulting nearly perfect shielding of pulsations and the substantial shielding of substorms from crust and mantle.

4.1.1.6 Morphology of geomagnetic variations

4.1.1.6.1 Solar daily variations (S)

S variations are defined as regular variations in local mean solar time. Depending on the degree of geomagnetic activity (see subsect. 4.1.1.7), Sq variations on quiet days (Q days) are distinguished from added S_D variations on disturbed days (D days), Fig. 2. S_D is found by subtracting from the observed S variation on D days that portion which could have been expected in the case of magnetic quietness.

S variations are derived from hourly mean values for a given geomagnetic field component (D, H, Z or X, Y, Z) by removing a linear trend from local midnight to local midnight. The remaining hourly means are averaged hour by hour of local time over the Q days of a certain interval (month, season) to obtain the mean Sq, and over the D days to obtain the mean S_D. The thus separated contributions to S have different global distributions, and are of different origin.

Sq variations: From rocket experiments it is known that they are mainly generated by currents in the ionosphere about 100 km above the ground. They are tangential and thus well resembled by equivalent currents as shown in Fig. 5. In addition poloidal magnetospheric currents exist which connect the two hemispheres along field lines.

The ionospheric Sq currents form two large loops on the day-lit side of the earth, which are symmetric to the equator during equinoxes. Their centers lie close to local noon in mid-latitudes. Viewed from space, the earth rotates under these ionospheric current loops, fixed in space by the position of the sun.

In the dynamo theory of Sq the driving electric fields are generated by motion of conducting matter in the ionosphere across field lines of the planetary field. The motion results primarily from thermally as well as gravitationally excited atmospheric tides. The size of Sq variations changes from maximum peak-to-peak amplitudes of 60 nT in the summer to minimum amplitudes of 20 nT in the winter. Both values refer to Sq variations in D (=magnetic east component) in mid-latitudes and average solar activity; about the same amplitudes apply to variations in H (=magnetic north component) in low latitudes (Fig. 6). In the immediate vicinity of the dip equator (line of zero inclination in Fig. 3e of subsect. 4.2.3) the H amplitude of Sq is three-fold increased by a local ionospheric current concentration known as equatorial electrojet (EEJ), Fig. 9.

On quiet days regular S variations become visible in the polar cap region inside the auroral zone. These S_q^P (P=polar) variations are not connected to the dynamo-driven Sq currents in middle and low latitudes, but arise from interaction of the steady solar wind with the magnetosphere.

In years of high sunspot number and thus high solar activity, Sq is twice as large as in years of low sunspot number (Fig. 7). Because tidal motion and solar heating can be assumed to be the same, the difference must come from an increased ionization of the high atmosphere when, in the yearly average, solar activity is greater.

For separate investigations of external and internal parts of Sq a spherical harmonic analysis is carried out with the Sq time harmonics: Let (θ, λ) denote the geographic coordinates of a point of observation; $\theta = 90° - \phi$ is its colatitude, ϕ its latitude, and λ its longitude. Let, for a given instant of time, X, Y, Z denote, respectively, the geographic north, east, and vertical downward component of Sq at this point. Their harmonic analysis from midnight to midnight in local time $T = t + \lambda$ (t=universal time) gives the Fourier coefficients A_m and B_m in expansions of the form

$$X(T, \theta) = \sum_{m=1}^{M} [A_m(\theta) \cos mT + B_m(\theta) \sin mT];$$

T is in angular measure ranging from $T=0$ to $T=2\pi$, one hour corresponding to $\pi/12$. In most analyses subharmonics up to M=4 are calculated, i.e. for periods of 24, 12, 8, and 6 hours, respectively. Tables with Fourier coefficients for S and L can be found in [Gup68].

The coefficients from a global network of observation points are expressed by series of spherical harmonics as described in subsect. 4.1.3.2. Usually this analysis is done after their conversion to universal time harmonics. Two sets of spherical harmonic coefficients (g_n^m, h_n^m) and (a_n^m, b_n^m) evolve from the analysis of horizontal and vertical components. By combining them separate sets of potential coefficients (γ_n^m, σ_n^m) and (c_n^m, s_n^m) are obtained for, respectively, the external and internal part of Sq as evident from eq. (6).

Fig. 5. Equivalent currents of solar daily variations Sq on quiet days, shown on global maps when local midnight is on the Greenwich meridian. The magnetic field of these currents reproduce the mean global Sq field for equinoxes, here for the September equinoxes 1957/58 of high solar activity. Fig. 5a is for the external part, Fig. 5b for the internal part, calculated for zero height and zero depth from spherical harmonic potential coefficients (cf. subsects. 4.1.1.4 and 4.1.4.4). Between contour lines flows a current of 25000 A and 20900 A, respectively. The numbers give the total current in the respective current system while the arrows indicate the direction of flow.
The causal connection between external and internal currents by induction is evident (cf. subsect. 4.2.2.1). The relative strength of internal Sq currents in the southern hemisphere may reflect the dominance of oceans in this hemisphere, allowing the unbounded development of an induced Sq current loop in the ocean. From [Par77].

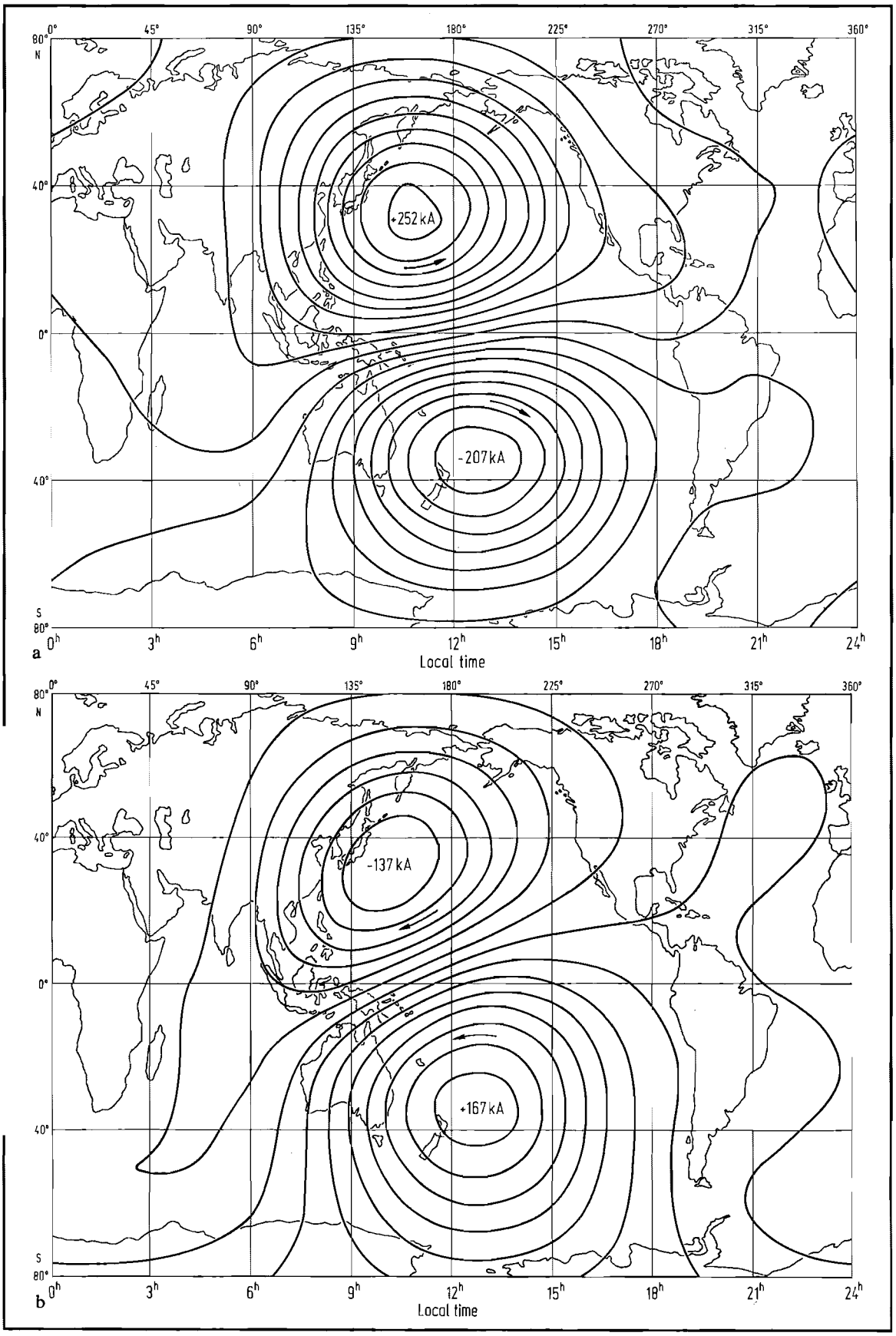
0°
45°
90°
135°
180°
225°
270°
315°
360°
80° N
40°
0°
40°
S 80°
+252 kA
-207 kA
0h
3h
6h
9h
12h
15h
18h
21h
24h
a
Local time
-137 kA
+167 kA
b
Local time

Schmucker

Table 2 presents potential coefficients from various analyses derived in the above manner. From the quoted sources those combinations of coefficients are extracted which describe Sq as a function of local time, i.e. the sinusoidal dependence on longitude and universal time is with $m(\lambda+t)$ as angular argument. See these sources for complete tables of coefficients. The meaning of the listed coefficients is as follows: Let V denote the Sq potential in local time. Then, with the notation as in eq. (3) of subsect. 4.2.3, but with a changed order of summations,

$$V(T,r,\theta)=R_E\sum_{m=1}^{M}\sum_{n=m}^{N}\left[\{\gamma_n^m\cos mT+\sigma_n^m\sin mT\}\left(\frac{r}{R_E}\right)^n+\{c_n^m\cos mT+s_n^m\sin mT\}\left(\frac{R_E}{r}\right)^{n+1}\right]P_n^m(\cos\theta). \quad (5)$$

Table 2 lists coefficients for $N=m+2$. In the case of the first two time harmonics, coefficients for $m+3$ are added because they contribute significantly. In fact, during equinoxes the 24 and 12 hour harmonics in local time are well described by the two terms $n=m+1$ and $n=m+3$ in direct consequence of the equator symmetry of the driving solar diurnal and semidiurnal tides [Win81].

The evaluation of eq. (5) with the coefficients in Table 2 yields the synthetic Sq potential for any chosen point outside the source region, from which equivalent currents can be calculated (cf. subsect. 4.1.3.4). Synthetic Sq variations as shown in Figs. 6···9 are derived from V by differentiation at $r=R_E$:

$$\begin{aligned}
X&=\frac{1}{R_E}\frac{\partial V}{\partial\theta}=\sum_m\sum_n\{g_n^m\cos mT+h_n^m\sin mT\}\frac{dP_n^m}{d\theta}\\
Y&=-\frac{1}{R_E\sin\theta}\frac{\partial V}{\partial T}=\sum_m\sum_n\{g_n^m\sin mT-h_n^m\cos mT\}\,mP_n^m/\sin\theta \quad (6)\\
Z&=\frac{\partial V}{\partial r}=-\sum_m\sum_n(n+1)\{a_n^m\cos mT+b_n^m\sin mT\}P_n^m
\end{aligned}$$

with

$$g_n^m=\gamma_n^m+c_n^m,\quad h_n^m=\sigma_n^m+s_n^m,\quad a_n^m=c_n^m-\frac{n}{n+1}\gamma_n^m,\quad b_n^m=s_n^m-\frac{n}{n+1}\sigma_n^m.$$

Note that differentiation with respect to longitude has been replaced by differentiation with respect to local time. For numerical evaluations observe that

$$\begin{aligned}
P_m^m&=f_m^m\sin^m\theta,\quad P_{m+1}^m=f_{m+1}^m\sin^m\theta\cos\theta\\
P_{m+2}^m&=f_{m+2}^m\sin^m\theta\left(\cos^2\theta-\frac{1}{2m+3}\right) \quad (7)\\
P_{m+3}^m&=f_{m+3}^m\sin^m\theta\left(\cos^3\theta-\frac{3}{2m+5}\cos\theta\right).
\end{aligned}$$

The scaling factor for quasi-normalized spherical functions, to which the coefficients in Tables 2 and 3 refer, is

$$f_n^m=\frac{(2n)!}{2^n n!}\sqrt{\frac{2}{(n-m)!\,(n+m)!}}.$$

Leading terms in the series expansion of Sq harmonics are terms with $n=m+1$ and $n=m+3$. They describe equivalent currents which are symmetric to the equator as to be expected at the time of equinoxes. During the solstices there are strong contributions from the first and third term with $n=m$ and $n=m+2$, accounting for the seasonal asymmetry of Sq.

Using only the leading terms, synthetic Sq variations are presented in Fig. 7 for high and low sunspot activity to demonstrate the quoted dependence of Sq on solar activity. Fig. 8 shows how well synthetic Sq variations with variable combinations of spherical terms resemble actual observations at a mid-latitude station.

S_D variations: They are connected with the influx of solar particles into the magnetosphere. In addition to these regular variations in local time, the particle influx produces fast irregular DP variations in the auroral zone and smoothed storm-time Dst and DS variations (subsects. 4.1.1.6.3 and 4.1.1.6.4). In contrast to Sq the amplitude of S_D depends strongly on latitude with maximum values of 100 nT in the auroral zone. As in Sq the source currents of S_D are fixed in space above the rotating earth.

The equivalent current system for the external part of S_D is dominated by a strong concentration of east-west currents in the auroral zone, eastward during the night and westward during the day. They are closed by widespread equivalent currents in opposite direction over the polar caps and mid-latitudes. Here S_D variations are responsible for long lasting departures in Z from the undisturbed level when, in the course of intense storms, the auroral zone moves south. The departures represent the vertical field of auroral east-west currents. Because of their local nature and long duration the compensation by an internal Z is incomplete.

Table 2. Spherical harmonic analysis of solar daily variations (S) in local time for years of, respectively, high and low sunspot numbers. The potential coefficients are listed for Schmidt's quasi-normalized spherical harmonic functions, eq. (5). In parenthesis the error in the last decimal (W: error in the last decimal of $(c^2+s^2)^{\frac{1}{2}}$ and $(\gamma^2+\sigma^2)^{\frac{1}{2}}$, respectively).

M: Malin's analysis for sunspot maximum with hourly means from 100 observatories. All days except the five most disturbed days of each month are used from July 1957 to December 1958 [Mal73, table A1]. Data base: Gupta-Chapman tables [Gup68].

P: Parkinson's analysis by seasons for the same sunspot maximum with hourly means from 64 observatories. The five most quiet days of each month are used during the equinoxes E (February···April and August···October), the northern summer N (May···July), and the southern summer S (November···January) between July 1957 and December 1958; [Par77, table VII s-v].

W: Winch's analysis for sunspot minimum with hourly means from 130 observatories. All days except the five most disturbed days of each month are used in the years 1964 and 1965; [Win81, table 8.10].

External part

m	n	γ	σ	γ	σ	γ	σ	γ	σ	γ	σ
		0.1 nT									
		M		P(E)		P(N)		P(S)		W	
1	1	8(7)	−11(7)	−4	−21	45	−35	−55	10	2	−10(3)
1	2	121(6)	−16(7)	125	−2	105	−19	118	−8	58	−20(2)
1	3	−11(5)	−2(5)	3	5	12	9	−18	8	−4	2(2)
1	4	−28(4)	−10(4)	−34	−7	−22	−9	−18	−12	−10	−4(1)
2	2	−4(3)	13(3)	12	16	−10	32	15	−20	0	11(2)
2	3	−59(3)	2(3)	−64	9	−52	15	−52	17	−28	9(1)
2	4	7(2)	2(2)	1	2	−12	3	9	0	−1	+1(1)
2	5	6 [1])	−3	2	−6	2	−1	4	−5	2	−2(1)
3	3	−0.4(12)	−5.3(13)	−3.8	−8.0	−2.2	−20.9	0.4	8.0	−1.1	−4.4(5)
3	4	20.8(11)	−5.5(11)	12.6	−9.6	10.4	−5.3	9.4	−8.4	9.8	−6.4(4)
3	5	−0.8(9)	−1.4(9)	−0.7	−1.4	0.7	−1.6	0	1.8	0.7	−1.9(4)
4	4	−0.1(6)	1.9(6)							0.9	1.5(2)
4	5	−3.9(5)	2.0(5)							−1.9	1.4(2)
4	6	0.3(4)	1.5(4)							−0.2	1.0(1)

[1]) Courtesy of Dr. Winch.

Internal part

m	n	c	s	c	s	c	s	c	s	c	s
		0.1 nT									
		M		P(E)		P(N)		P(S)		W	
1	1	−3(5)	−12(5)	−11	−8	12	−19	−22	5	1	−5(2)
1	2	45(5)	−6(5)	61	−1	48	−8	53	−4	23	−7(2)
1	3	4(4)	2(4)	−2	−3	0	1	−12	−1	1	−1(2)
1	4	−15(4)	8(4)	−10	10	−3	7	−7	11	−2	5(1)
2	2	2(3)	5(3)	8	9	0	21	7	−9	0	4(1)
2	3	−24(3)	8(2)	−28	10	−25	12	−21	15	−10	9(1)
2	4	2(2)	−1(2)	1	2	−1	2	2	−1	0	−1(1)
2	5			2	−5	−1	−1	4	−4	0	0(1)
3	3	−0.3(10)	−1.4(10)	−3.1	−2.9	−3.0	−11.2	0.8	3.9	−2.0	−1.5(5)
3	4	7.8(10)	−5.7(10)	0.8	−7.7	2.9	−3.9	−0.7	−5.6	4.3	−4.8(4)
3	5	−0.9(8)	−0.1(8)	0.1	−0.2	−0.3	−2.0	0.7	1.2	−0.6	0.2(3)
4	4	1.0(5)	0.5(5)							0.5	0.4(2)
4	5	−1.2(5)	1.7(4)							−0.6	1.2(2)
4	6	0.0(4)	0.6(4)							0.2	0.4(1)

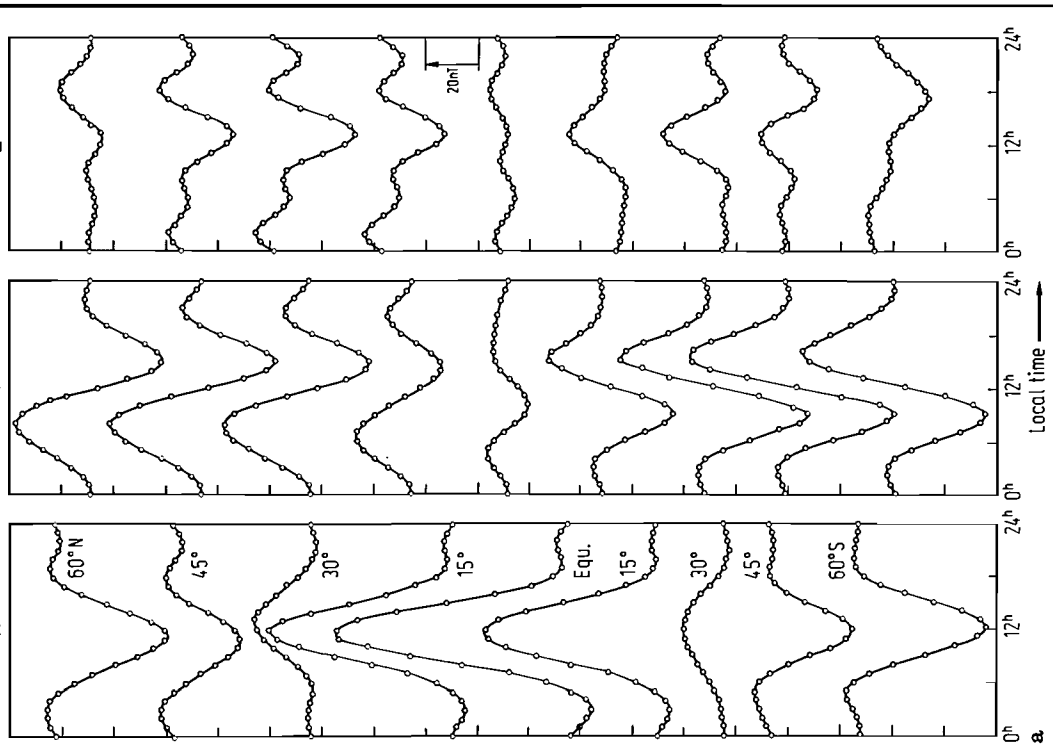

Fig. 6a. Calculated solar daily variations Sq on quiet equinoctial days in local time from midnight to midnight between 60° south and 60° north. Hourly values in X (north component), Y (east component), and Z (vertical downward component) are from a time-harmonic and spherical harmonic synthesis, evaluating eqs. (6) with the potential coefficients P(E) in Table 2. They represent the mean Sq during equinoxes in years of maximum sunspot number. See Fig. 7 for the variability of Sq with solar activity and Fig. 4 in subsect. 4.2.2 for a separate presentation of external and internal parts.

Fig. 6b. Calculated solar daily variations Sq during the northern summer, using the spherical harmonic coefficients P(N) in Table 2. See Fig. 6a for further explanation.

Fig. 6c. Calculated solar daily variations Sq during the southern summer, using the spherical harmonic coefficients P(S) in Table 2. See Fig. 6a for further explanation.

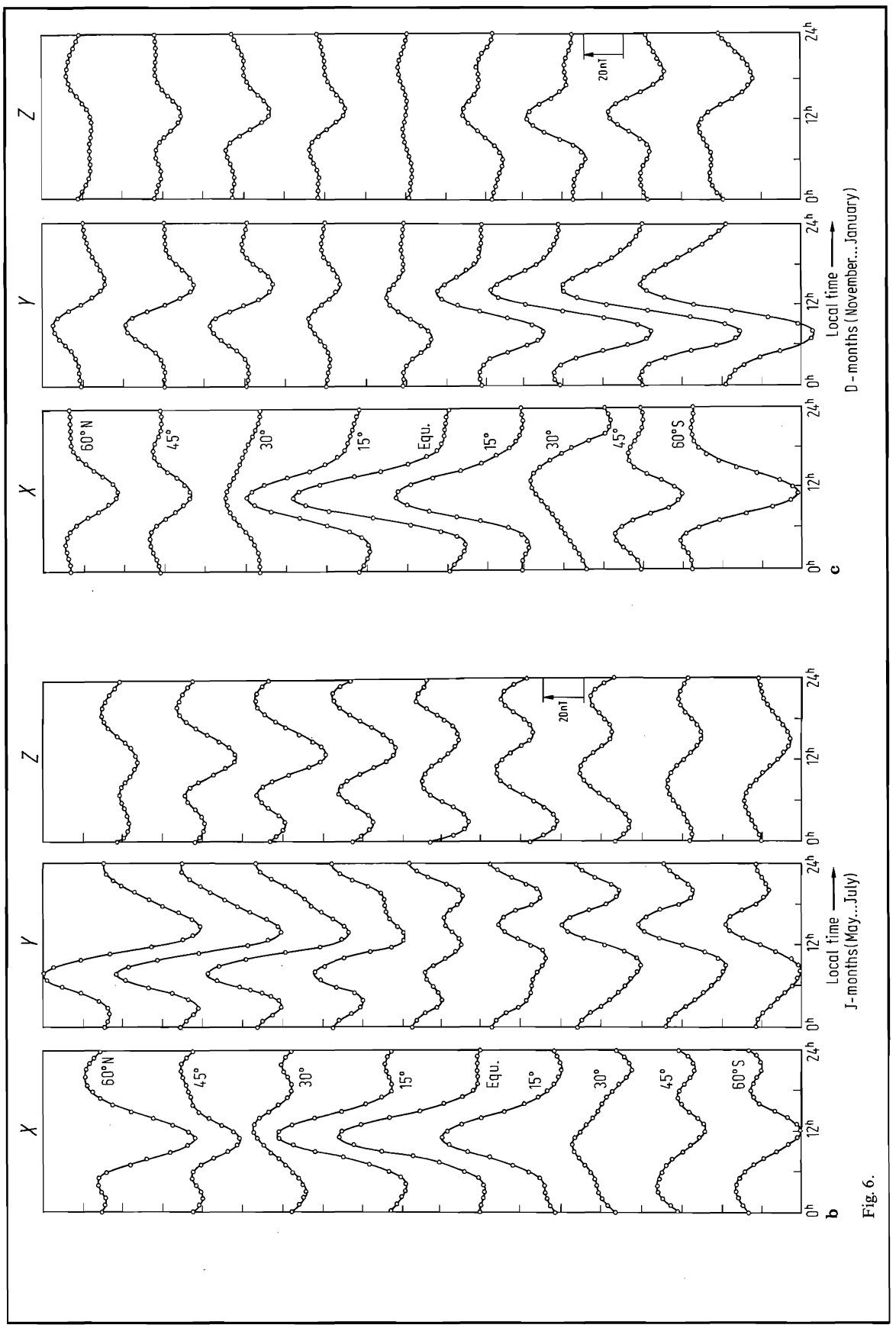
X
Y
Z
60°N
45°
30°
15°
Equ.
15°
30°
45°
60°S
20nT
0h
12h
24h
Local time
J-months (May...July)
D-months (November...January)
b
c

Fig. 6.

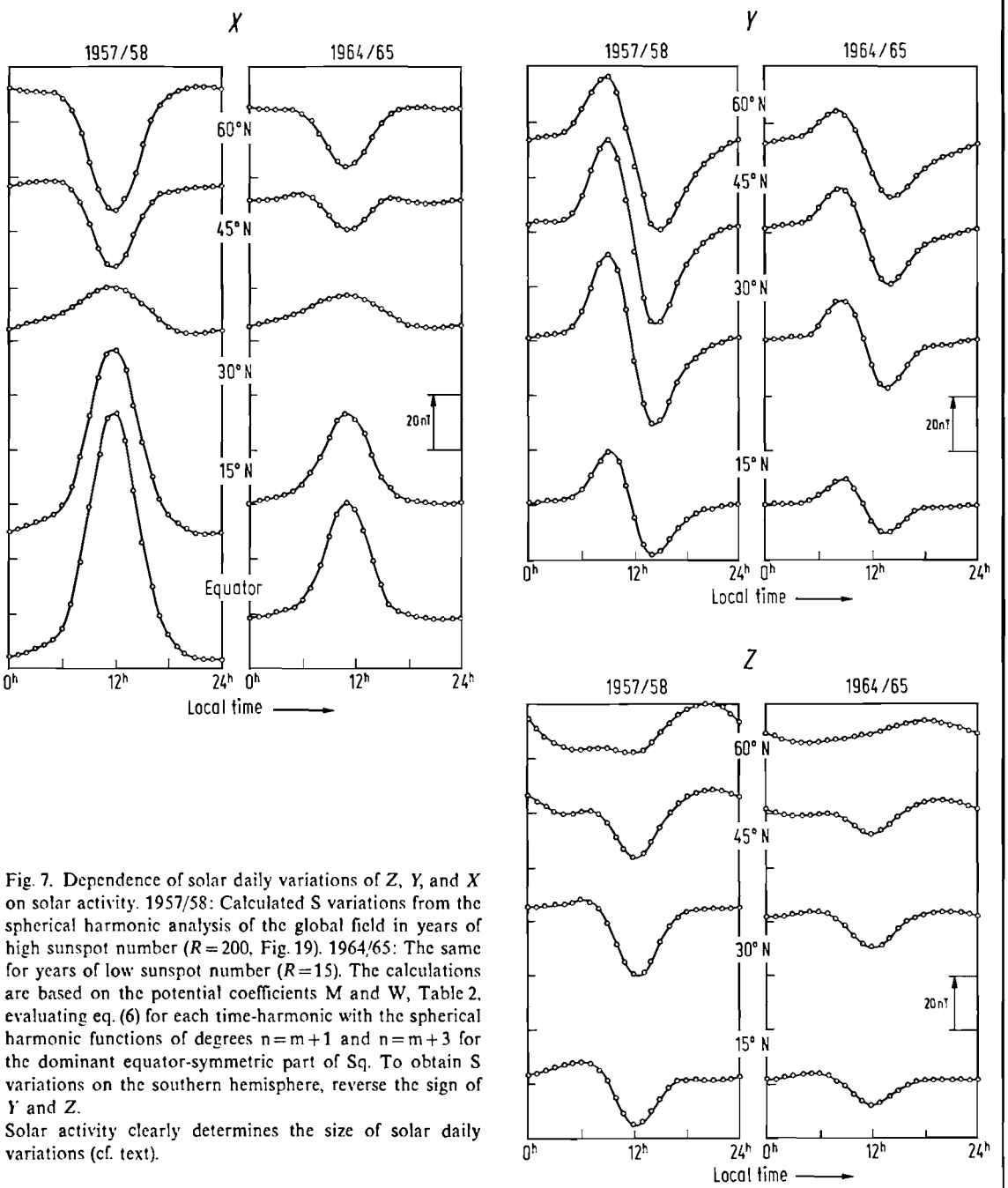

Fig. 7. Dependence of solar daily variations of Z, Y, and X on solar activity. 1957/58: Calculated S variations from the spherical harmonic analysis of the global field in years of high sunspot number ($R=200$, Fig. 19). 1964/65: The same for years of low sunspot number ($R=15$). The calculations are based on the potential coefficients M and W, Table 2, evaluating eq. (6) for each time-harmonic with the spherical harmonic functions of degrees $n=m+1$ and $n=m+3$ for the dominant equator-symmetric part of Sq. To obtain S variations on the southern hemisphere, reverse the sign of Y and Z.
Solar activity clearly determines the size of solar daily variations (cf. text).

Fig. 8. Comparison of observed and calculated solar daily variations of Z, Y, and X in local time. Open circles: Mean Sq variations at Fürstenfeldbruck (FUR; 11.28° E, 48.17° N) in March 1958 according to Price and Stone's tables [Pri68]. Full circles: Calculated Sq variations from a time-harmonic and spherical harmonic synthesis according to eq. (6), using the complete set of potential coefficients P(E) in Table 2. Triangles: The same, but including in the synthesis only the leading spherical harmonic of degree $n=m+1$ for the m-th time harmonic.

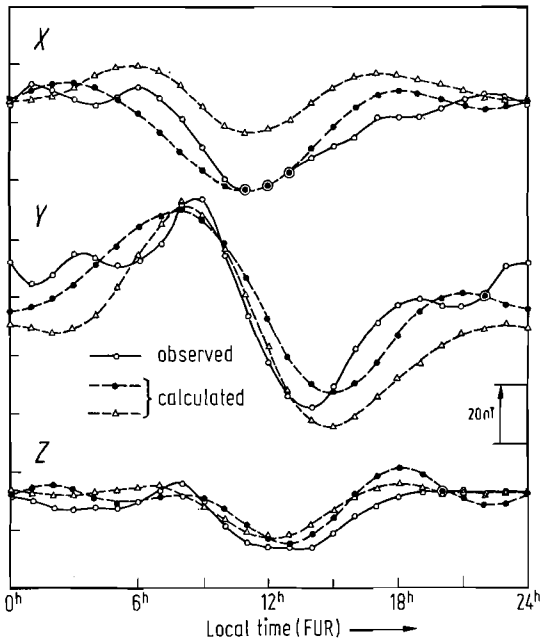

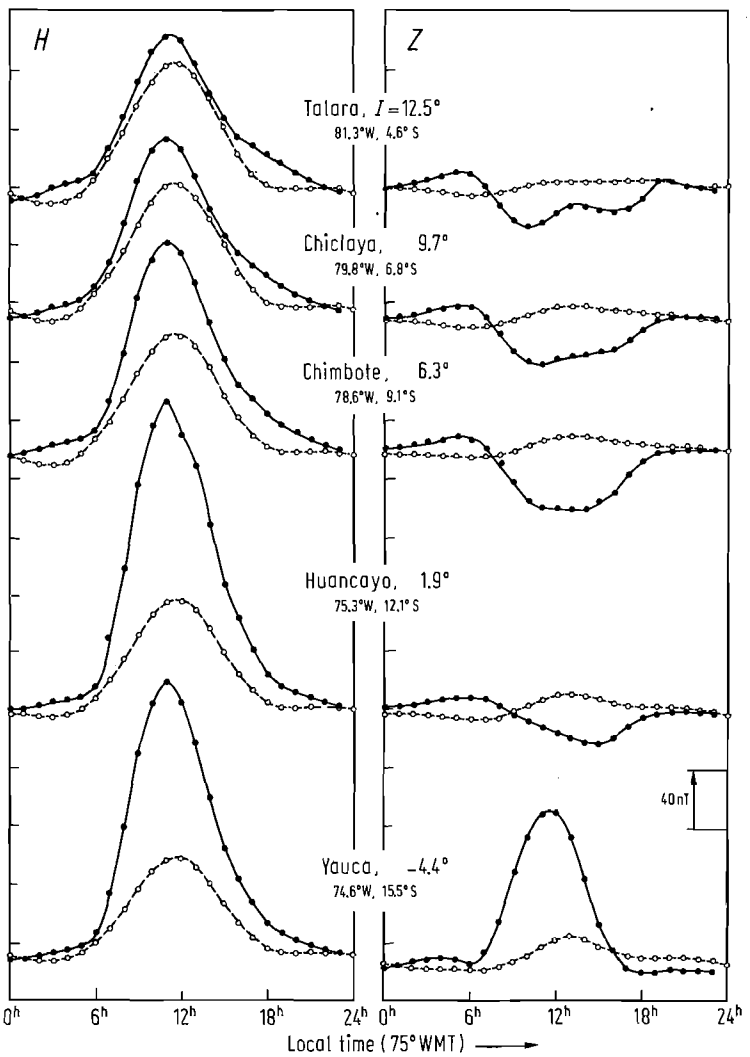

Fig. 9. Electrojet enhancement of solar daily variations of H and Z along the dip equator (=line of zero magnetic inclination). Solid curves: Mean Sq variations from 20 quiet equinoctial days 1958/59, observed with a chain of temporary observatories across the dip equator in Peru (I= angle of magnetic inclination). Hourly means from [For61, Tables 9···23]. Dashed curve: Calculated Sq variations for the respective latitudes from a time-harmonic and spherical harmonic synthesis with the potential coefficients P(E) in Table 2. The more than twofold increase of daily variations in H near zero dip and the appearance of deviating Z variations of opposite signs north and south of the dip equator indicate the existence of an overhead current concentration, known as equatorial electrojet EEJ, following within the global Sq current system the dip equator on the day-side. Rocket experiments have verified its ionospheric origin.

4.1.1.6.2 Lunar daily variations (L)

L variations are regular geomagnetic variations which arise from lunar tides in the oceans and atmosphere. If tidal currents with velocity $\boldsymbol{v}$ move across field lines of the earth's planetary field, electric fields $\boldsymbol{v} \times \boldsymbol{B}$ are generated. They drive electric currents in the well conducting seawater and in the ionosphere. The motion-induced currents produce electromagnetically induced currents within conducting layers of the earth. The superimposed magnetic field of all currents is observed as lunar daily variations L.

Ionospheric and oceanic contributions to L can be separated because only the oceanic L depends exclusively on local mean lunar time τ. The leading lunar tide (M_2) has a period of half a lunar day. Hence, $f(\tau)=\sin(2\tau+\alpha)$ is the dominant time factor for motion-induced currents with τ in angular measure, $\tau=\pi/12$ corresponding to 1 hour in lunar time. This is also the time factor for the oceanic L.

The changing conductivity σ in the ionosphere during the day produces for the ionospheric L an additional dependence on local mean solar time T. It has the approximate form of Chapman's phase law

$$L(T,\tau)=\sum_{m=0}^{4} l_m \sin\{(m-2)\,T+2\tau+\varphi_m\},$$

L standing for any of the magnetic components or the potential. This is the time dependence of the product $f(\tau)\cdot\sigma(T)$ with

$$\sigma(T)=\sum_{m=0}^{2} c_m \sin(m\,T+\gamma_m)$$

describing the solar time dependence. Writing the difference of local solar and lunar time as phase of the moon, $v=T-\tau$ ($v=0$: new moon), the phase law reads

$$L(T,v)=\sum_{m=1}^{4}[A_m \cos(m\,T-2v)+B_m \sin(m\,T-2v)]. \tag{8}$$

The term with $m=0$ and a period of half a lunar month is difficult to observe and here omitted.

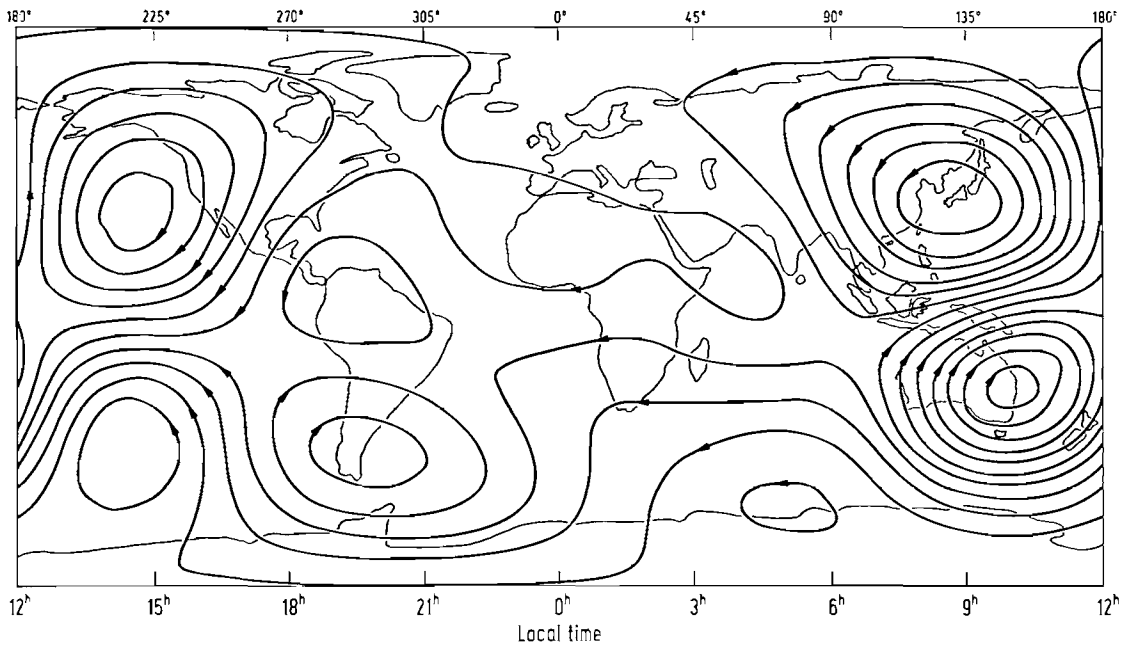

Fig. 10. Equivalent currents of lunar daily variations L, shown on global maps when local midnight is on the Greenwich meridian and the moon overhead at noon (new moon, $v=0$). The currents are for the external part of L, calculated for zero height from spherical harmonic coefficients for 1957/58, which are years of maximum sunspot number. Between contour lines flows a current of 1000 A. Two separate current loops exist on the day-lit side of either hemisphere. Cf. the equivalent currents for S, Fig. 5, and text, from [Mal73].

The phase law is the basis for the analysis of ionospheric L variations at a given site and lunar phase. A global analysis of the Fourier coefficients in eq. (8) as functions of longitude and latitude yields as in the case of Sq (cf. subsect. 4.1.1.6.1) sets of external and internal spherical harmonics. They are listed in Table 3, but again only for the dominating local-time-dependent part of L. See the cited references for extended tables of spherical harmonics. See subsect. 4.1.1.6.1 for instructions how to derive from the tabulated potential coefficients ionospheric L variations at a given site.

L variations are in general too small to be noticeable in the magnetic records without analysis of long time series. Maximum peak-to-peak amplitudes (Y in mid-latitudes and X in low latitudes) are 3 nT (Fig. 11). Solar activity almost doubles L variations, which, as in the case of S, shows the overall increase of ionospheric conductivity by enhanced solar UV radiation, including weak X-rays.

Equivalent currents for the external part of L variations involve two separate loops on either hemisphere separated by the local noon meridian (Fig. 10). The current pattern changes slightly with changing lunar phase. The doubling of current loops in comparison to Sq reflects the fact that the motion-induced source field currents of L arise exclusively from gravitational tides.

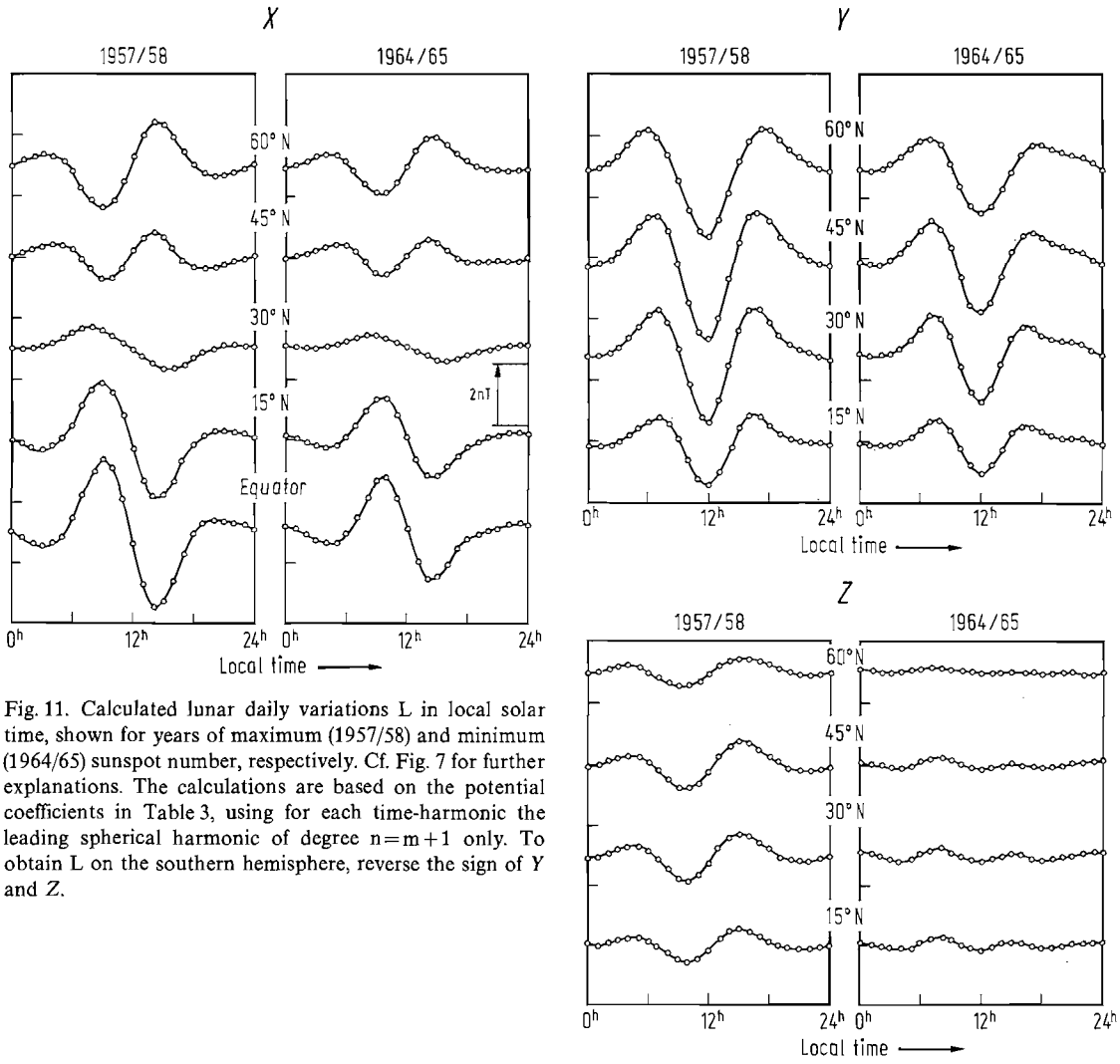

Fig. 11. Calculated lunar daily variations L in local solar time, shown for years of maximum (1957/58) and minimum (1964/65) sunspot number, respectively. Cf. Fig. 7 for further explanations. The calculations are based on the potential coefficients in Table 3, using for each time-harmonic the leading spherical harmonic of degree $n=m+1$ only. To obtain L on the southern hemisphere, reverse the sign of Y and Z.

Table 3. Spherical harmonic analysis of lunar daily variations (L) for years of, respectively, high and low sunspot number. The potential coefficients refer to the ionospheric part of L according to the phase law, eq. (8), for the semi-diurnal lunar tide, i.e. their time factors are $\cos(mT-2\nu)$ and $\sin(mT-2\nu)$, respectively, for the phase ν of the moon. They are listed for Schmidt's quasi-normalized spherical harmonic functions, eq. (5). In parenthesis the error in the last decimal (W: error in the last decimal of $(c^2+s^2)^{\frac{1}{2}}$ and $(\gamma^2+\sigma^2)^{\frac{1}{2}}$, respectively).
M: Malin's analysis for sunspot maximum 1957/58;
W: Winch's analysis for sunspot minimum 1964/65. See legend to Table 2 for detailed information on the data base.

External part

m	n	γ	σ	γ	σ
		0.01 nT			
		M		W	
1	1	−8(6)	−3(6)	−3	−1(2)
1	2	−2(6)	−34(6)	1	−17(1)
1	3	1(3)	2(3)	0	3(1)
2	2	10(7)	4(7)	3	6(2)
2	3	3(6)	50(6)	−4	25(2)
2	4	−1(5)	−9(5)	0	2(2)
3	3	−1.7(29)	−4.1(29)	−2.4	−4.2(10)
3	4	−3.5(28)	−18.6(28)	−0.7	−13.4(9)
3	5	−0.7(21)	4.2(21)	−3.2	−2.7(8)
4	4	0.1(12)	0.2(12)	0.8	0.5(4)
4	5	−0.3(11)	3.9(11)	0.1	4.2(4)
4	6	0.5(9)	−1.4(9)	0.6	0.4(3)

Internal part

m	n	c	s	c	s
		0.01 nT			
		M		W	
1	1	−3(5)	4(5)	−2	3(1)
1	2	−3(5)	−14(5)	0	−13(1)
1	3	−2(4)	4(4)	1	−2(1)
2	2	−3(6)	−5(6)	0	−7(2)
2	3	8(6)	21(6)	−3	21(2)
2	4	2(5)	0(5)	−4	−4(1)
3	3	0.9(26)	−1.5(27)	−1.4	−2.4(9)
3	4	−3.7(26)	−8.9(26)	−4.1	−9.2(8)
3	5	−0.6(20)	1.8(20)	0.0	1.3(7)
4	4	−0.1(11)	−0.3(11)	0.2	−0.5(4)
4	5	0.4(10)	2.2(11)	0.9	2.4(3)
4	6	0.5(9)	0.1(8)	0.6	−0.3(3)

4.1.1.6.3 Polar magnetic storms and substorms

Magnetic storms are irregular variations due to an interaction of the magnetosphere with an intermittently enhanced stream of particles from the sun. They involve a large range of amplitudes and periods from a few minutes to a few hours. The following special types of variations are observed: Solar flare effects (sfe) occur when intense solar wave emission from flares increases the ionospheric conductivity and intensifies Sq variations on the day-side, usually for ten or twenty minutes (Fig. 2). Solar flare effects are indicators of solar activity, but as a rule do not precede individual storms.

Between 18 and 26 hours after leaving the sun, erupted plasma reaches the orbit of the earth. Interaction on its way with the steady solar wind develops a shock wave propagating through interplanetary space. Its impact on the magnetosphere initiates a magnetic storm, usually with a globally observed sudden storm commencement (ssc). Its cause may be visualized as a fast compression of the magnetosphere. The ssc is always positive in the magnetic north component H, reaching up to 200 nT (Figs. 2 and 13a).

The following main phase of the storm is likewise globally observed with rapid magnetic field fluctuations, most intense in the auroral zones and here, at most times, of little spatial coherency (Fig. 13a). Within minutes the field may change at a given site by, say, 500 nT, but no comparable change may be observed a few 100 km away. There is a well established correlation with the display of auroral lights.

The auroral zone is the zone of the most frequent occurence of auroral lights as seen from the surface of the rotating earth. It forms a circle of 19 degrees radius, slightly excentric with regard to the geomagnetic poles. Hence, its ground position varies during the day. At local midnight the auroral zone is typically 23° away from the geomagnetic pole, at local noon 15°. During very intense storms the auroral zone moves further away from the geomagnetic poles. The auroral zone is to be distinguished from the auroral oval, the zone of instantaneous auroral lights as seen from space.

The distinction of auroral latitudes arises from the fact that field lines of the planetary field which intersect here the earth's surface connect the high atmosphere to regions in the magnetosphere which are filled up after storm begin with solar particles from the by-passing solar wind and from existing particles in the plasma sheet. Charged particles move in the magnetosphere most easily along field lines and thus are guided into the auroral zones on both hemispheres (Fig. 1).

Magnetic ground observations show that up and down going branches of such field-aligned magnetospheric currents are closed in the ionosphere of the auroral zone by east-west polar electrojets PEJ, variable in length, position, and strength. Their magnetic field is observed as DP variations, more specifically as DP1 variations. They die away with increasing distance from the auroral zone towards higher and lower latitudes. In the equivalent current representation the PEJ is eastward where DP1 variations occur before local midnight, and westward where they occur after local midnight (Fig. 12a). The closure by presumably magnetospheric currents appears as wide-spread return current over polar caps and mid-latitudes.

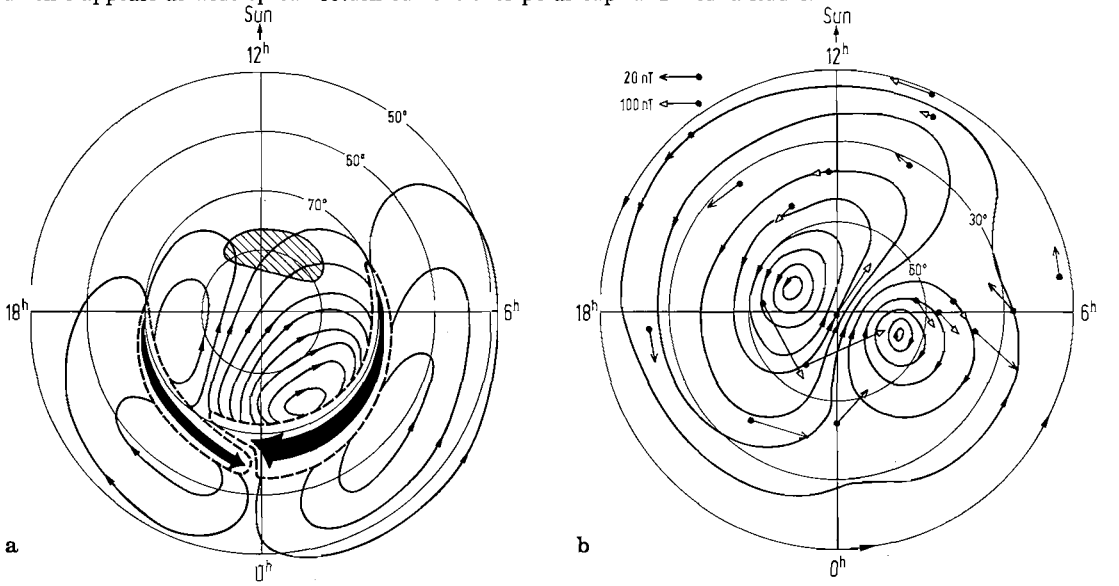

Fig. 12. Equivalent currents for the external part of disturbed polar DP variations as seen from the geomagnetic pole on the northern hemisphere and calculated for zero height. See subsect. 4.1.1.4 for the assumed ratio of external to internal parts. Meridians are identified by their hour in local time. See Fig. 13 for records with DP variations.
(a) DP1 equivalent current model. Concentrated currents, denoted as polar electrojets PEJ, flow in the night-side auroral zone of 67 degrees latitude eastward before midnight and westward after midnight. The direction of flow is shown by arrows. Both currents meet at midnight at the Harang discontinuity which can move into the evening sector during intense substorms as indicated. They correspond to true currents in the lower ionosphere at 100 km height in contrast to the shown return currents outside the auroral zone which possibly model the field of true currents in the magnetosphere.
(b) DP2 equivalent current model, derived from averaged magnetic ground observations, with 50000 A between flow lines. The vectors represent the external part of the horizontal disturbance field, rotated clockwise by 90 degrees to indicate the direction of overhead currents. Two current loops exist with centers in the auroral zone and widespread return currents in low latitudes, directed eastward at the equator. Note the similarity of DP2 and Sq equivalent currents in the afternoon sector (Fig. 5), from [Nis68].

Irregular variations in low latitudes which can be correlated with magnetic activity in high latitudes are ascribed to a second type of DP variations denoted as DP2. Their equivalent currents are similar to those of Sq. directed from high to low latitudes in the morning sector, and from low to high latitudes in the evening (Fig. 12b). At least near to the dip equator true DP2 currents flow in the ionosphere because an equatorial electrojet-enhancement is observed on the day-side.

DP1 variations which last for a few hours only and begin without ssc accompany a short-lived influx of particles into the high atmosphere initiating, even in times of relative magnetic quietness, polar substorms. In mid-latitudes they produce from early evening to early morning smooth temporary departures from the undisturbed level for one or two hours. They are known as bays (Fig. 13b). Their equivalent currents are similar to those of DP1 at the respective hour of local time.

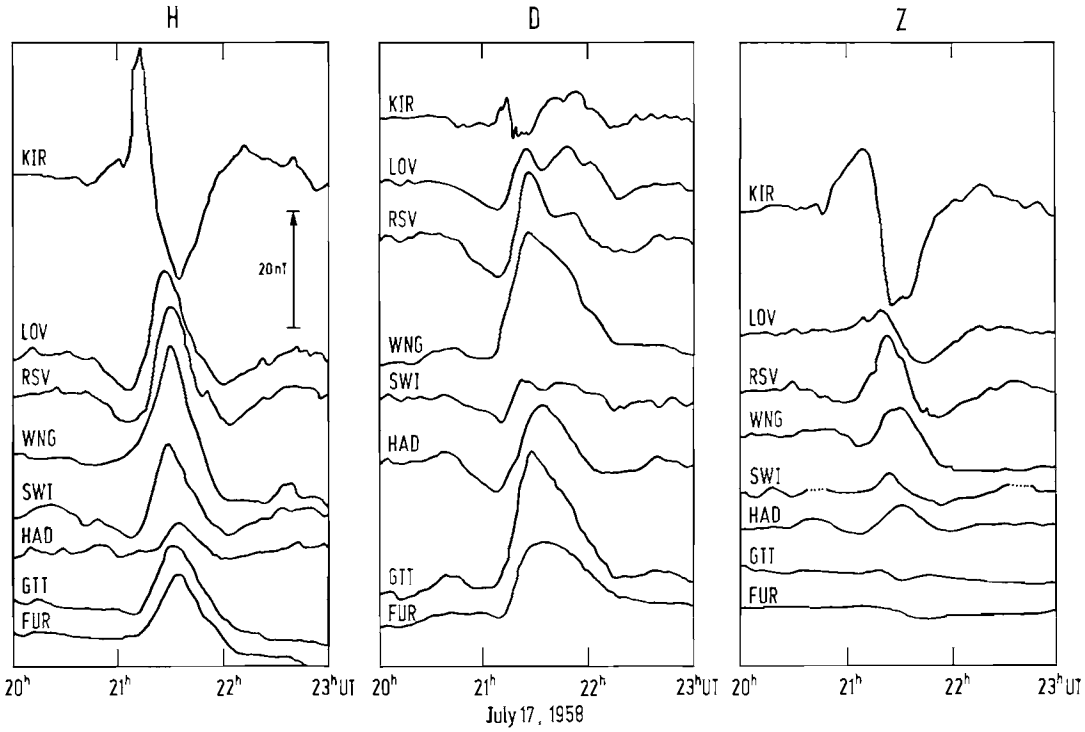

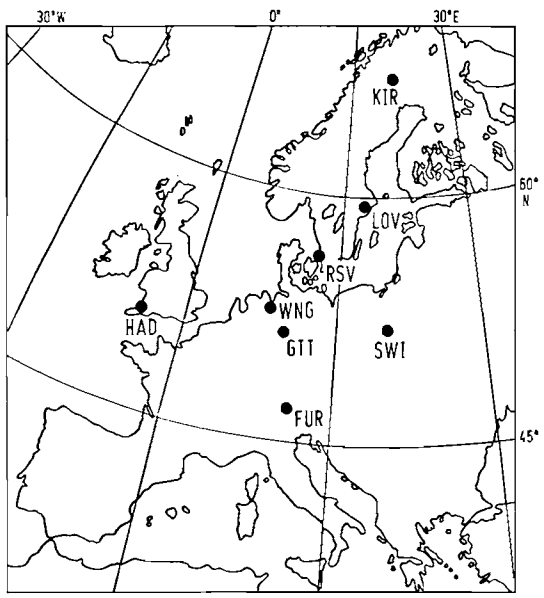

Fig. 13a ▶

Fig. 13b. Simultaneous records of a polar substorm in Northern Scandinavia, observed further south as an isolated bay disturbance. Vertical lines are hour marks. The substorm occurred in the late evening of a quiet day ($Kp \leqq 3-$). See Fig. 13a for further explanations, but note that *D* is here the magnetic east component of the disturbance.
Except for the station Kiruna (KIR) in the auroral zone *H* and *D* variations are well correlated with a clear amplitude reduction toward south. Deviating variations at Hartland (HAD) and Swider (SWI) reflect the longitude dependence of substorms, i.e. their dependence on local time. Strong parallel *H* and *Z* variations at Kiruna could indicate that an electrojet of varying strength flows just south of this station. The comparatively small *Z* amplitudes outside the auroral zone arise from an almost complete compensation of external and internal *Z* fields due to induction. If the earth were a perfect insulator, *Z* variations at least as strong as those in *H* and *D* would be observed. For names and locations of stations, see also subsect. 4.3.2, Table 1.

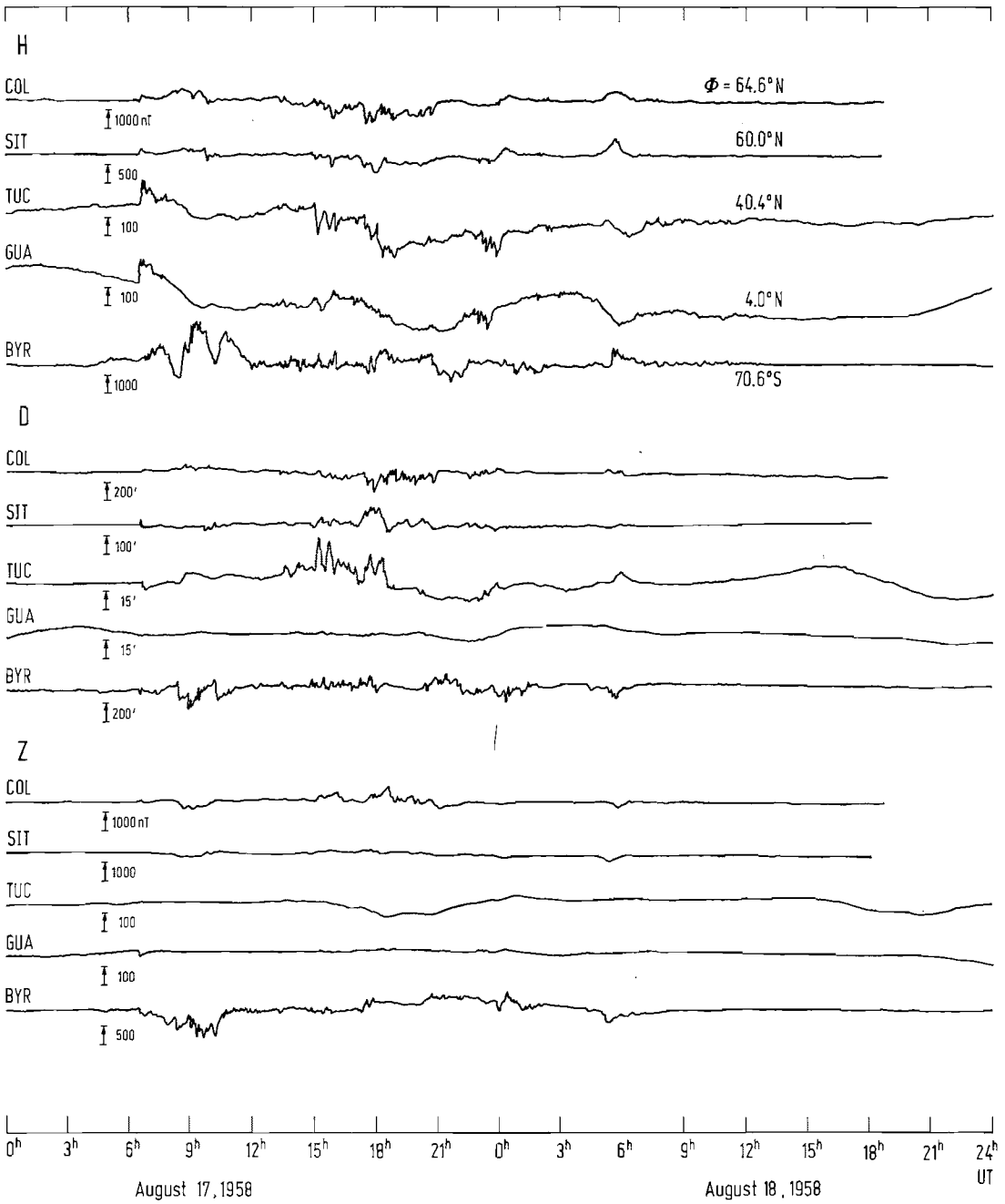

Fig. 13a. Simultaneous observations of a magnetic storm ($Kp \leqq 7+$), in the northern auroral zone (COL: College/Alaska), in high latitudes south of the auroral zone (SIT: Sitka/Alaska), in mid-latitudes (TUC: Tucson/Arizona), at the equator (GUA: Guam), and in the southern auroral zone (BYR: Byrd Station/Antarctica). Φ = geomagnetic latitude. The magnetic records are for the horizontal intensity H, the declination D, and the vertical downward intensity Z. Note the difference in scales necessary to compensate the tenfold increase of storm-time variation in the auroral zones. See Table 1 in subsect. 4.2.3 for exact locations of the observatories. The storm begins with a globally observed sudden storm commencement (ssc) and lasts for 2 days. The H depression due to Dst ring current variations is clearly visible in low latitudes. Note the strong DP variations in the southern polar region which have no correspondence on the northern hemisphere. H and D variations in high and low latitudes are well correlated while those in the auroral zone are mostly incoherent. Note also the strong D variations in mid-latitudes which are missing at the equator. The small storm-time amplitude of Z variations in high and low latitudes indicates a nearly complete compensation of external and internal parts. Strong Z variations in the auroral zone arise from local jet fields with incomplete compensation.

4.1.1.6.4 Smoothed storm-time variations Dst and DS

During the main phase of magnetic storms a globally observed depression begins in the magnetic north component H. Near to the equator it may move H down to 200 nT below its pre-storm level. Similar, but smaller departures are observed in the vertical component Z, positive north, and negative south of the equator (Fig. 13a). Maximum departures are reached already within a day after storm begin, while the smooth return to the pre-storm level lasts for many days (Fig. 14). No lasting departures are observed in the magnetic east component D.

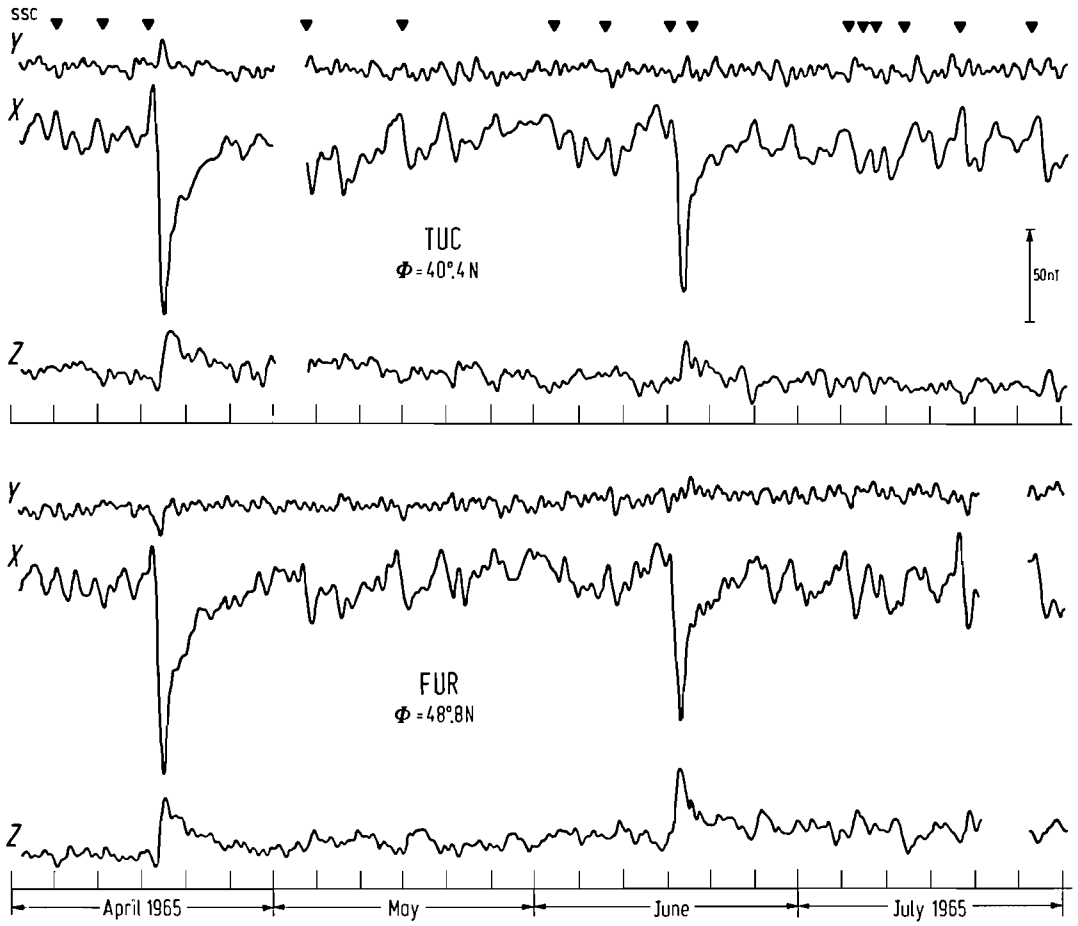

Fig. 14. 4-months section of smoothed storm-time variations shown for the east component Y, north component X, and vertical component Z, at two mid-latitude observatories TUC (Tucson/Arizona; 110.8° W, 32.3° N) and FUR (Fürstenfeldbruck/Bavaria; 11.3° E, 48.2° N); Φ = geomagnetic latitude. Triangles indicate confirmed sudden storm commencements ssc, IAGA Bulletin No. 12 t2 (subsect. 4.1.4.3). Daily variations have been removed with a low-pass filter (cut-off period 32 h), secular variations with a parabolic trend polynomial. The section is from a year of minimum sunspot number (cf. Fig. 19).
Two ssc's are followed by storms (Kp 8− and Kp=7o, respectively) with well developed Dst ring current variations, evident from the downward deflection in X and the concurrent upward deflection in Z. They are clearly visible for about ten days after the ssc because these storms are followed by periods of exceptional quietness. For a non-conducting earth these deflections would have been of comparable size in mid-latitudes. The observed $Z:X$ deflection ratio α of 1/4 indicates an internal to external potential ratio $Q=(1-\alpha)/(2+\alpha)$ of 1/3; cf. subsect. 4.2.2.2.2. See Fig. 3, subsect. 4.2.2, for a separation of the Dst potential into internal and external parts. Each of the remaining ssc's is accompanied by a short-lived Dst phase, contributing to a continuous sequence of ultraslow variations in the earth's magnetic field. Note the visible correlation which this Dst continuum displays in X and Z between the two widely separated sites of observation, while ultraslow Y variations appear to have a longitude-dependent phase. Their correlated part can be attributed to DS (cf. Fig. 15).

The recovery phase of magnetic storms occurs globally in universal time, reckonned in storm time t_{Dst} after storm begin (ssc). For its analysis fast DP variations in higher latitudes are removed by smoothing, likewise Sq variations. The remaining smoothed storm-time variations are split into a truly universal-time-dependent part Dst and a local-time-dependent part DS by taking averages along circles of latitude.

The external part of Dst resembles closely the uniform field of a westward circular current in the equatorial plane of geomagnetic coordinates known as equatorial ring current ERC. According to satellite observations the ERC can be attributed to the drift and gyration of charged particles in the magnetosphere several earth's radii away, oscillating along planetary magnetic field lines. The drift results from the inhomogeneity of the planetary field, electrons drifting westward and protons drifting eastward.

DS variations, denoted as disturbed local time inequality, reflect an only partial closure of the equatorial ring current during the first days of storm time. They disappear when magnetic quietness returns (Fig. 15).

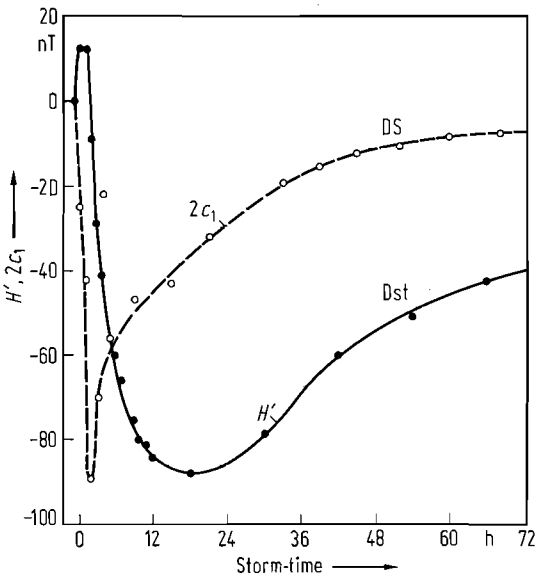

Fig. 15. Separation of smoothed storm-time variations into equatorial ring current variations Dst and disturbed local time inequalities DS for three days of storm-time. Full and open circles represent average values from the analysis of those 74 great storms in the years 1902···1945 which have started with a sudden storm commencement (ssc). Records of six observatories between 21° and 42° latitude have been used. Dst values approximate the time-varying ring current field in the geomagnetic north component H' for 30° geomagnetic latitude. The DS curve is the peak-to-peak fundamental amplitude $2c_1$ in H' when, for a given instant of universal time, DS along circles of 30° latitude is expressed by Fourier series $\sum_m c_m(\cos m\lambda + \phi_m)$, λ in angular measure ($2\pi \triangleq 1$ day).
After a few hours of storm-time the zonal, only on universal time dependent Dst field exceeds DS, from [Sug60].

4.1.1.6.5 Solar cycle variation

When from long magnetic records at a given site the secular variation of the planetary field is removed, minute but significant oscillations remain which show a persistent quasi-periodicity of about 11 years (Fig. 16). They are well correlated on a global scale and have a clear relation to the sunspot cycle of 11 years.

In years of low sunspot number the departure of the magnetic north component H from the smoothed level of the planetary field is positive, during years of high sunspot number negative. The departure of the vertical component Z is opposite in sign north and in the same sense as H south of the equator. These departures in H and Z correspond to an equatorial westward ring current ERC which in the long-term average varies in strength with solar activity. But there exist also significant and longitude-dependent departures in the magnetic east component.

Together they describe the solar cycle variations of the earth's magnetic field. They add a contribution of primarily external origin to secular changes of the field. Various attempts have been made to remove solar cycle effects from annual means of observatory data to obtain unbiassed estimates of secular variations which are free of external contaminations. Should equatorial ring currents be a permanent characteristic of the magnetosphere and thus exist also in times of minimum solar activity, a small quasi-uniform field of external origin would be superimposed on the measured planetary surface field at all times (Fig. 17).

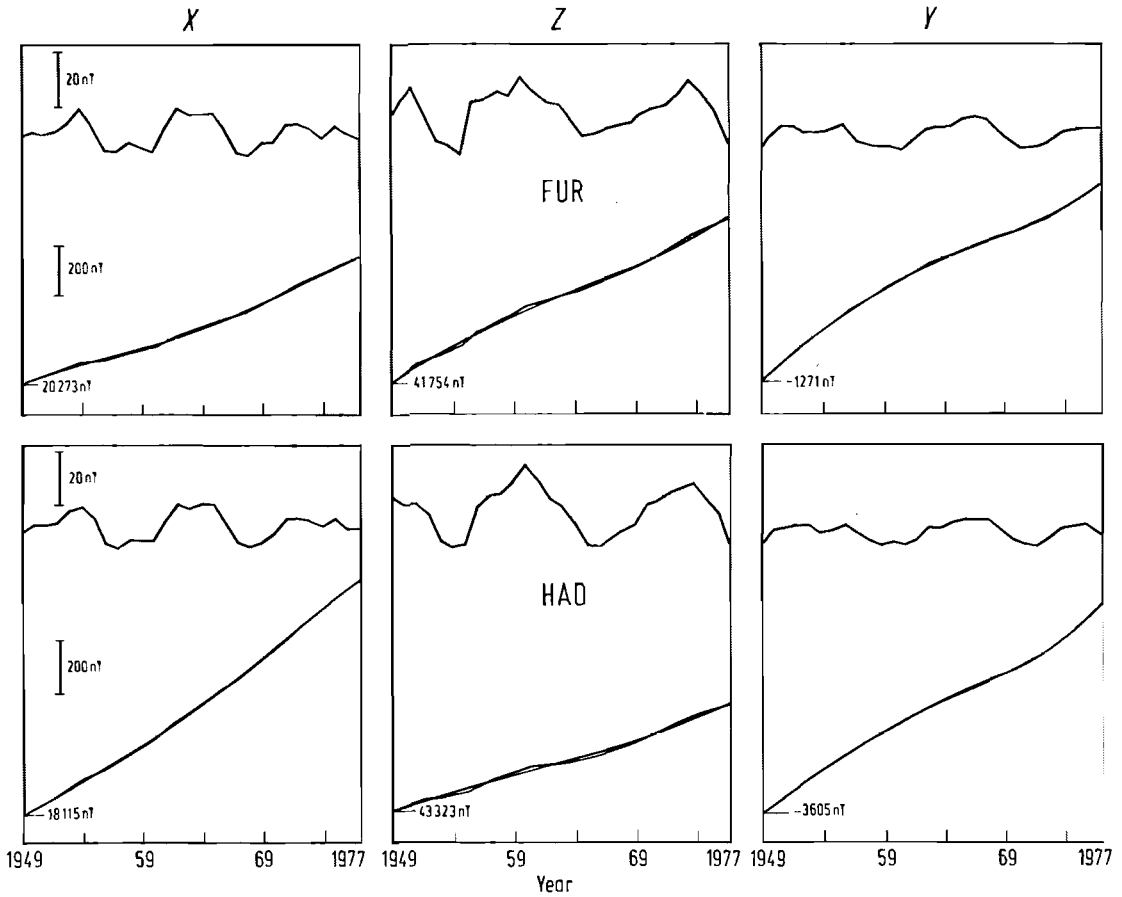

Fig. 16. Solar cycle variations and the underlying trend of secular variations within 28 years according to observations at two European sites, HAD (Hartland/England; 4.5° W, 51.0° N) and FUR (Fürstenfeldbruck/Bavaria; 11.3° E, 48.2° N). The lower presentation shows for each observatory the secular change of annual mean values of rectangular field components X, Z, and Y; at the left their absolute values for 1949 in [nT]. A cubic trend polynomial fitted to these secular changes is superimposed. See for example Z at HAD for discernible departures between annual means and trend polynomial (the smoother of the two curves). These departures are displayed in the upper presentations on a 10-fold increased scale. They reveal an 11-year quasi-periodicity. The good correspondence between the departures of the two observatories proves their reality. They are attributed to the overall change of the mean equatorial ring current field within the solar cycle of varying sunspot number (cf. Fig. 19 and text). About equal amplitudes of X and Z in mid-latitudes indicate that solar cycle variations are basically of external origin. But see subsect. 4.2.2.2 for a possible small internal part by induction at great depth. Note that clearly resolved solar cycle variations in Y are not consistent with the concept of a simple equatorial ring current source.

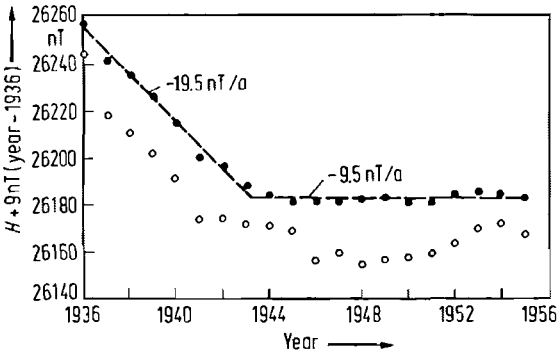

Fig. 17. Secular variation of the horizontal intensity H, observed at Tucson/Arizona (110.8° W, 32.3° N). To compensate for the secular change after 1943, 9.5 nT/a are added from 1937 onward. Open circles: Annual mean values obtained from midnight values of magnetically quiet days. Full circles: horizontal intensity of the earth's magnetic field derived from the annual means by removal of solar cycle variations. These variations are clearly resolved in the annual means. An additional contribution constant in time of external origin of about 10 nT which has been found to exist even in years of minimum sunspot number (1943, 1954) has been added to the annual values corrected for solar cycle variations. Note that this procedure reveals a discontinuous change of secular variations in the year 1943 as indicated by the cross-over between the two dashed straight lines characteristic of the smoothed secular change in H before and after the year 1943.

4.1.1.6.6 Pulsations and electromagnetic wave emissions

Geomagnetic pulsations are rapid oscillations in the period range from fractions of a second to several minutes. They occur intermittendly as regular, sometimes modulated, sinusoidal pc pulsations and as irregular pi pulsations. Their amplitudes decrease with decreasing period. For a period of 30 seconds a typical amplitude is 1 nT in mid-latitudes, 10 nT in high latitudes. Slow pulsations with periods of 5 minutes and longer may have amplitudes of some tens of nT in the auroral zone (Fig. 18). See Table 1 for a subdivision of regular pulsations according to their period.

Mid-latitude pulsations occur well correlated over large distances of 1000 km and more. Very rarely giant pulsations pg are observed, but only locally over distances of less than 1000 km. The occurence of pc pulsations is local-time-dependent and to some extent controlled by geomagnetic activity. Substorm variations begin often with pi pulsations.

The spectrum of ELF emissions shows spikes at 7 Hz and multiples. They are interpreted as Schumann cavity resonance of electromagnetic fields between the solid earth and the ionosphere, both nearly perfect conductors for rapid field oscillations. Toward higher frequencies the spectrum is extended up to 20 kHz by VLF emissions. Their source are electromagnetic wavelets propagating through the magnetosphere and impinging on the ionosphere. Thunderstorm-incited wavelets are observed as whistlers in the same frequency band [joh61].

4.1.1.7 Geomagnetic indices

Geomagnetic indices have the purpose to classify the various types of geomagnetic variations with regard to their strength in given intervals of time. For irregular variations indices characterize the range, defined as difference of maximum deviations above and below the undisturbed Sq level, for the component which has the greatest difference within the interval.

K indices are a local quasi-logarithmic measure for the range of 3 hour intervals in universal time. They have 10 classes between $K=0$ (magnetic quietness) and $K=9$ (magnetic storm). For selected standard stations in mid-latitudes the upper threshold for $K=0$ corresponds to a range of 5 nT, the lower threshold for $K=9$ to 500 nT.

Kp indices are a global quasi-logarithmic measure of magnetic activity in 3 hour intervals, available in tabular form since 1932 [Bar62]. They are derived from the K indices for a selection of observatories with proper weights for latitude and local time. The planetary Kp index is scaled in 28 classes from 0o, 0+, 1−, 1o, ··· to 9o. Based on Kp the five quietest Q days and the five most disturbed D days are identified for each month (Fig. 19).

Ap indices are a daily linear measure of magnetic activity. A formal translation is the equivalent mid-latitude amplitude of irregular variations, in units of [nT] equal to twice the Ap index. The Ap index is derived from the planetary Kp index. Its conversion to a linear scale defines a new 3 hour index ap. The daily mean of ap in universal time is Ap (Fig. 20).

Cp indices are a daily quasi-logarithmic measure of magnetic activity derived from the linear 3 hour indices ap after conversion to a logarithmic scale. They replace formerly used C_i indices based on a visual inspection of magnetograms.

Various indices have been introduced to monitor the auroral amplitude of DP variations, the equatorial amplitude of Dst variations. See the references [Sie71] and [may80] for detailed information on these and other geomagnetic indices.

Short-term changes of Cp and Ap indices reflect the tendency of strong geomagnetic activity to return after 27 days, i.e. after a full rotation of the sun, long-term changes the interdependence of geomagnetic and solar activity (Fig. 20). But this interdependence is clearly visible only during the descending branch of the sunspot cycle. No simple relation exists between sunspot number R and activity index Ap, which excludes sunspot activity as the immediate source of geomagnetic activity.

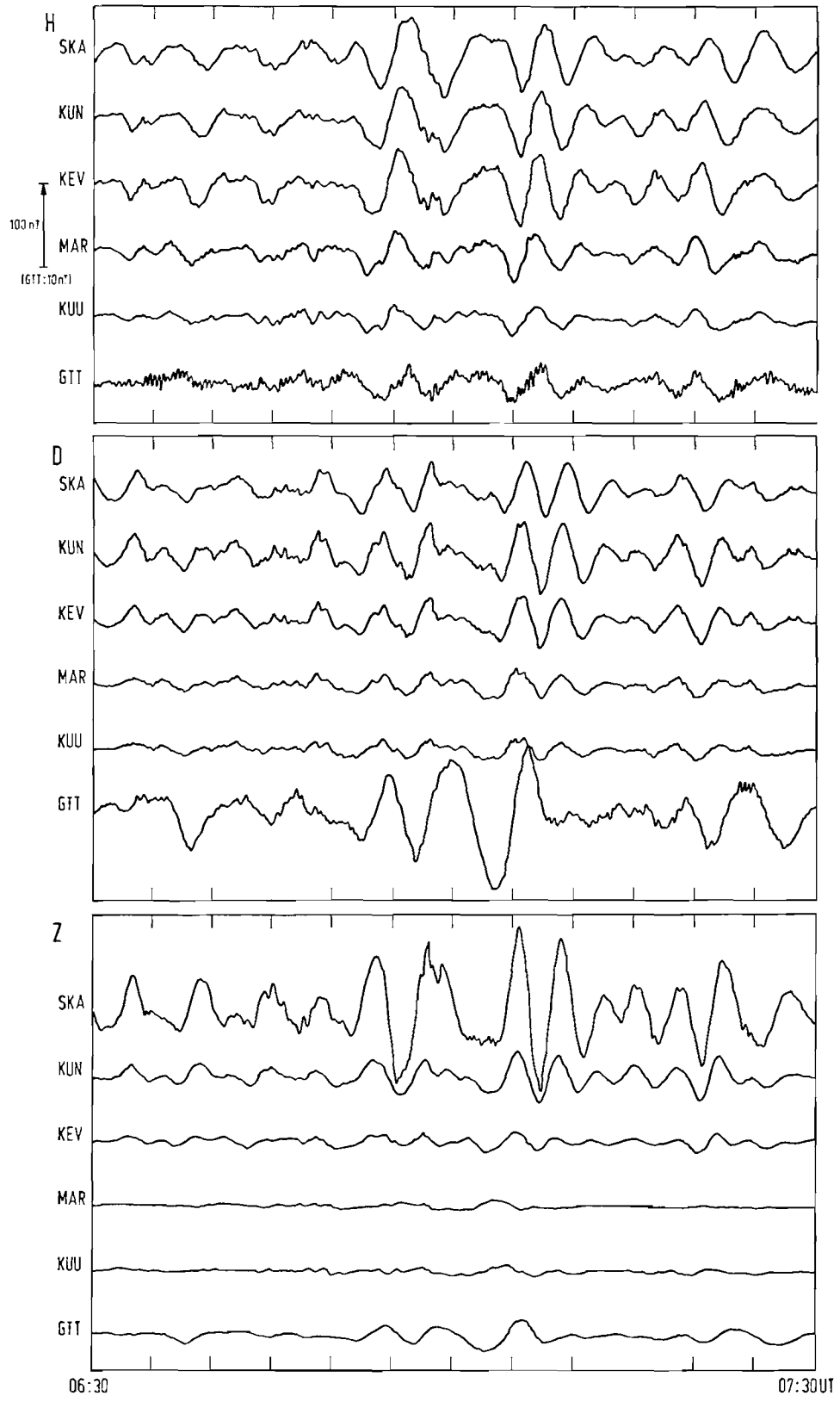
H
SKA
KUN
KEV
100 nT
MAR
(GTT: 10 nT)
KUU
GTT
D
SKA
KUN
KEV
MAR
KUU
GTT
Z
SKA
KUN
KEV
MAR
KUU
GTT
06:30
07:30 UT
August 31, 1978

Fig. 18.

Fig. 18. Simultaneous records of slow geomagnetic pulsations from a chain of five sites across the auroral zone in northern Scandinavia. Note that *D* is the magnetic east component of the disturbance field. The geomagnetic latitude of the most northern station Skarsvag (SKA) is 67.6°, of the most southern station Kuusamo (KUU) 62.4°. For comparison records from the mid-latitude site Göttingen (GTT) (52.3°) are added. The northern sites of observation follow the 110° geomagnetic meridian (25···30° E in geographic coordinates); the geomagnetic longitude of GTT is 93.7°. All records have been corrected for instrumental response and show the true field fluctuations. Note the tenfold reduced scaling for GTT.
Highly correlated pulsations are visible throughout the entire 1 hour record section. In the polar electrojet region at 67° (SKA, KUN, KEV) maximum pulsations of nearly 100 nT are observed in the horizontal magnetic north and east components *H* and *D*, respectively. Amplitudes are reduced southward (MAR, KUU). For mid-latitudes the reduction is more prominent in *H* than in *D*. Note that the increased sensitivity at Göttingen brings out superimposed fast pulsations, which evidently are not intensified at the same rate toward north. Pronounced *Z* variations at SKA at the North Cape of Scandinavia are a local coast effect due to induced currents in the ocean, from [Glas84].

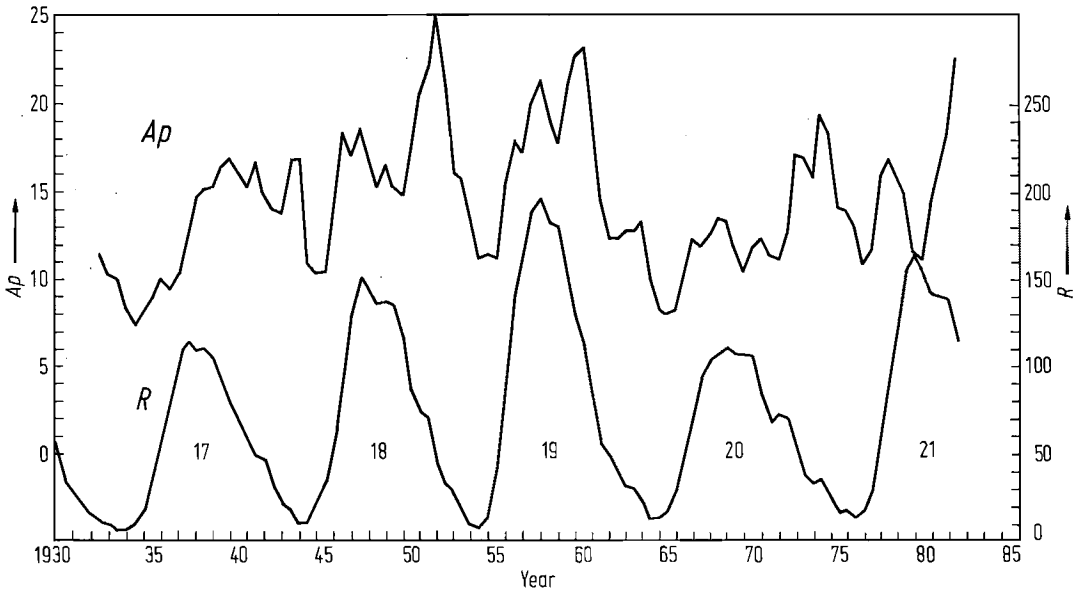

Fig. 19. Variations of the *Ap* index of geomagnetic activity (cf. subsect. 4.1.1.7) and of the relative sunspot number *R* during the last five solar cycles 17···21, demonstrating the causal connection between both phenomena. The clearly developed 11-year cycle of solar activity is also visible in the long-term variation of geomagnetic activity, here expressed by the averaged daily linear measure *Ap*. In particular, sunspot maxima of varying height (cf. solar cycles 19 and 20, for instance) are well reproduced in varying degrees of maximum geomagnetic activity. But note the time lag between extrema in both series. Maximum geomagnetic activity is reached only several years after maximum solar activity, while the minima of both curves nearly coincide, from [Sie71, Fig. 9]; revision and extension to the year 1982 courtesy of Dr. Siebert.

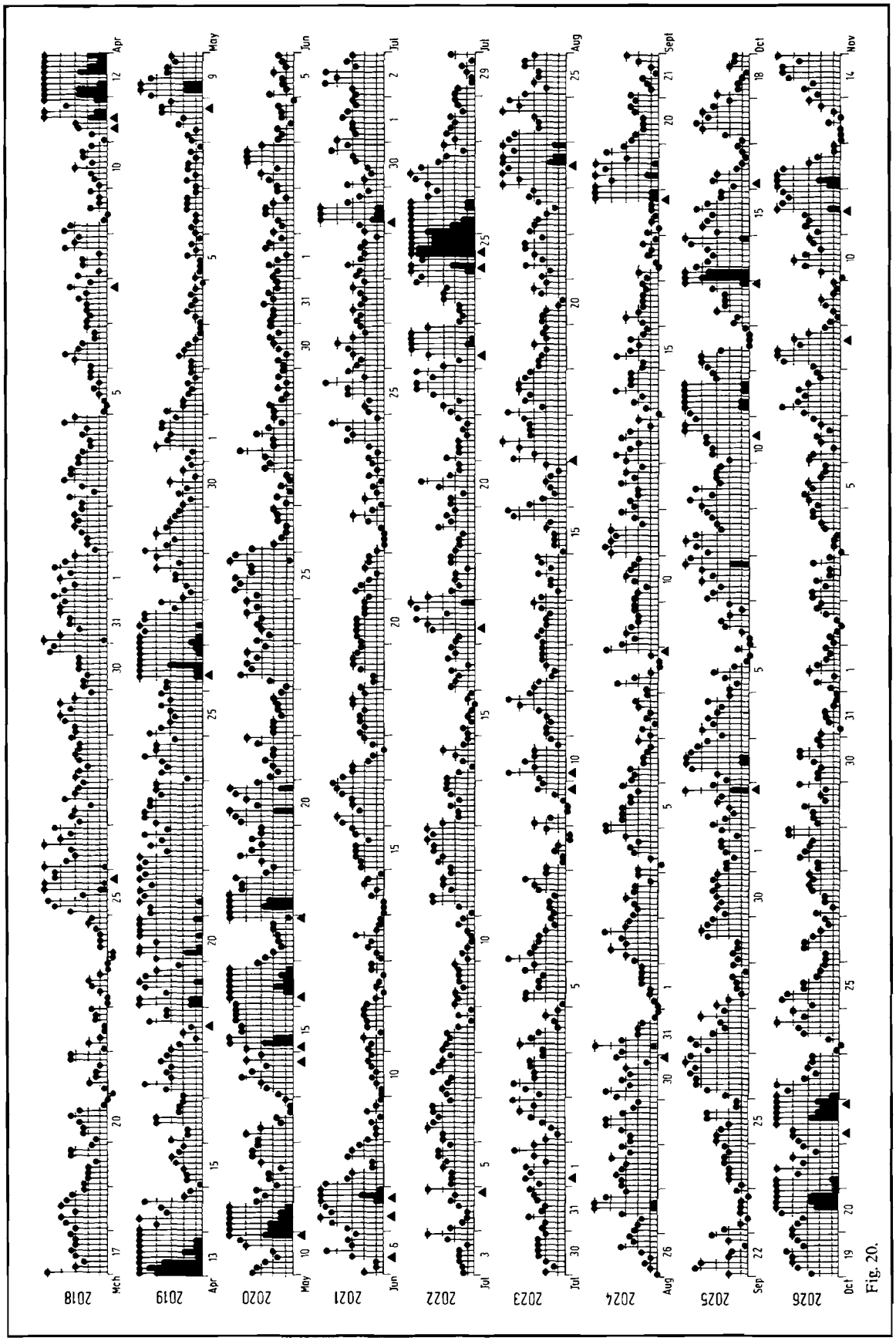

Fig. 20.

Schmucker

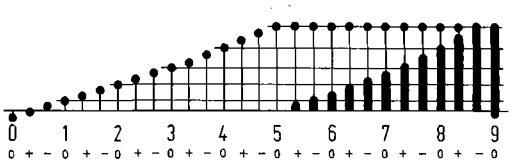

Fig. 20. Bartel's musical diagram of the planetary Kp index of geomagnetic activity (cf. subsect. 4.1.1.7), arranged according to nine full rotations of the sun in the year 1981. The rotations are numbered at the very left. Triangles indicate sudden storm commencements ssc, even though some of them are not followed by increased activity. The tendency of magnetic storms to reoccur after a full rotation of the sun is visible at left and right margins of the diagram. 1981 has been a year of more than average magnetic activity, following a sunspot maximum in the year 1979 (Fig. 19).

4.1.2 Internal part of the earth's magnetic field

4.1.2.1 Sources of the internal part

Three types of sources within the earth contribute:

(i) a hypothetical planetary dynamo driven by convective motion in the outer fluid portion of the metallic core;

(ii) a variable magnetization of crustal rocks above the Curie isotherm of magnetite;

(iii) electromagnetic induction of currents by fields of external origin in oceans, crust, and mantle.

The main internal contribution is ascribed to the core field, i.e. to dynamo currents in the outer core. Their magnetic field has a dominating dipole term, even when the field is extrapolated downward to the surface of the core (subsect. 4.1.2.3). In the long-term average the dipole axis appears to coincide with the axis of rotation, while the polarity of the dipole undergoes reversals on a geological time scale. See subsect. 4.3.1 for details.

Near to the poles the surface flux density of the core field is about 60000 nT which gives the earth's core an equivalent magnetization of 440 A/m. This is also the equatorial sheet current density of equivalent currents flowing eastward in the surface of the core along circles of constant (geomagnetic) latitude Φ with sin Φ as latitude factor. See subsect. 4.2.4 for physical conditions and processes in the core which are required by the existence of a planetary dynamo throughout the earth's history.

Time variations of the core field are observed, but only on a secular scale. Faster variations, should they occur in the source region, do not reach the earth's surface because of electromagnetic screening by conducting matter in the mantle. Likewise unobservable are structural details of the core field because of the great depth of their origin. In addition, only the tangential electric modes of dynamo currents contribute to the observable magnetic surface field.

Contributions to the internal part from magnetized rocks are in contrast spatially incoherent and comparatively small. They add a crustal field of mostly local and anomalous character which exceeds 1000 nT only sporadically at exceptional places. See subsect. 4.2.1 about details and subsect. 4.1.2.4 for the distinct difference in the multipole spectrum from core and crust.

Contributions from induced currents are also small, in general less than 100 nT, and are connected to time-varying fields. See subsect. 4.1.1 for the external source field, and subsect. 4.2.2 about the internal induced field. The currents are well explained by electromagnetic induction in electrically conducting layers of crust and mantle, at short periods with a substantial contribution from oceans and sedimentary basins. The slowest and most deeply penetrating variations induce currents downward to 1000 km depth.

4.1.2.2 Spherical harmonic analysis of the geomagnetic field 1835 to 1980

The smooth appearance of the core field in time and space at the earth's surface makes it well adapted for a representation by converging series of spherical harmonics. The coefficients of these series are derived from field values X (geographic north component), Y (geographic east component), or Z (vertical down component) in a global network of grid points. They refer to the field at a certain instant of time, denoted as epoch. See subsect. 4.1.3.2 for details of this analysis.

Contributions from fluctuating fields are removed from the data by taking time averages of observatory records, usually annual means, and by applying appropriate corrections to instantaneous field determinations. This may not eliminate ultraslow variations completely such as solar cycle variations (subsect. 4.1.1.6.5). Thus, annual means may contain small contributions which are external in origin and change with geomagnetic activity.

Local anomalies of crustal origin are removed by spatial smoothing, usually by reading off grid values from world charts of the magnetic field drawn on the basis of many individual observations. But note that any smooth field contributions from the crust on a global scale will be attributed falsely to the core field.

Table 4 contains spherical harmonic coefficients of degree n=1 (dipole) and degree n=2 (quadrupole) for six selected epochs between 1835 and 1979.85. See [fan59, III], [Bar78] and in particular [McD67] for complete tables of coefficients and details about their determination. Tables 7 and 8 in subsect. 4.2.3 list coefficients of two of the most recent analyses for 1975 and 1980. Tables 11 and 12 in subsect. 4.2.3 add a complete list of dipole coefficients and geomagnetic pole positions, using all available determinations with $N \geqq 4$ since 1835.

The entries in Table 4 are as follows: L is the number of grid point values from which the spherical harmonics have been determined by a least-squares analysis; N is the maximum degree and order of the series expansion, i.e. the total number of coefficients is $N \cdot (N+2)$. There exists a truncation error due to the use of field values at discrete points (cf. subsect. 4.1.3.2). Therefore coefficients from expansions with different N are not strictly comparable. Numerical experiments show that truncation errors are not important for degrees smaller than about $N-2$.

The analysis is carried out with a network of grid points on a sphere, say, every ten degrees in latitude and longitude. The data base are records from an increasing number of observatories, now more than 100 (Table 2 in subsect. 4.2.3), instantaneous measurements at a few thousand repeat stations, magnetic surveys on land and sea, and, since epoch 1965., airborne observations.

The most recent analyses incorporate satellite observations and thus avoid effects from local anomalies and from the non-uniform distribution of observation points at the surface. But because the satellite moves through the source region of geomagnetic time variations, their elimination is problematic. Therefore observations on only two exceptionally quiet days ($Kp \leqq 1+$) were used in the analysis quoted for epoch 1979.85. In contrast all earlier analyses combine field observations of many years with problematic reductions to a common epoch.

The code in the next column identifies the method of analysis, noting that the analysis of more than one field component may yield redundant determinations of the potential coefficients. See subsect. 4.1.3.2, last paragraph, for details. The code XYZ indicates a combined least-squares analysis of all components, XY a combined analysis of the horizontal components, Z an analysis of the vertical component. Assuming an internal origin of the field, the listed coefficients for Z, a_n^m and b_n^m, should be identical with those derived from X and Y, g_n^m and h_n^m. The code XY, Z implies two separate analyses of horizontal and vertical components, the code X, Y, Z three separate analyses of all components with an attempted removal of non-potential parts of the field. In the last two cases external and internal parts are formally separated. The coefficients listed in Table 4 are those of the internal part.

All coefficients refer to an equivolumetric earth's radius $R_E = 6371$ km (MAGSAT 6371.2 km). In the analysis of ground data, the oblateness of the earth is disregarded except for the analysis epoch 1865. For epochs 1922., 1945., and 1965. the accuracy of the analysis can be estimated from the discrepancies between coefficients derived either from horizontal or vertical components. Presumably they are not due to the neglect of external parts, but arise from data imperfections, i.e. from errors of measurement, residual effects of local anomalies, and time variations.

For epoch 1965. the following errors of the XY analysis are quoted: 5···7 nT for dipole and quadrupole terms, 2···4 nT for those of higher degrees. The errors of the Z analysis are about twice.

Only the 1979.85 MAGSAT analysis gives in $\gamma_1^0 = 20.4$ nT a significant zonal external coefficient of degree n=1. It agrees well with the expected existence of a steady and uniform equatorial ring current field (subsect. 4.1.1.6.4) during the time of observations. Because the satellite data of this analysis are instantaneous with minimum contribution from crustal anomalies and time variations, the MAGSAT coefficients may be regarded as the most accurate ones to date. See Table 7 in subsect. 4.2.3 for a list of coefficients up to degree and order n=10 of epoch 1980. But note that even the best available set of spherical harmonics reproduces the true surface field only within tens of nT.

A test with 54 time-reduced observations in the United States (50 repeat stations and 4 observatories) gives mean deviations of 22(137) nT in X, −33(99) nT in Y, and −33(201) nT in Z when compared with the synthetic field from MAGSAT coefficients epoch 1979.85 [Lan80]. The values in parenthesis are standard deviations and show the important influence of very local anomalies at some of the chosen sites.

A comparison of the Gauss coefficients in Table 4 reveals a remarkable steady change with time in the last 145 years. They are largest for the zonal terms g_1^0 and g_2^0, +2360 nT, or +16.3 nT/a, for the axial dipole, and −2505 nT, or −17.3 nT/a, for the axial quadrupole. For the three dipole terms together the rate of change is 17.4 nT/a. It appears that this change has accelerated in recent decades from 16.1 nT/a between the years 1835··· 1965 to 27.6 nT/a between the years 1965···1980.

These rates of change refer to the flux density of the dipole field at the respective geomagnetic equator (cf. eq. (7) in subsect. 4.2.3.1.2). To obtain the corresponding change of the dipole moment in units of [Am^2], multiply the quoted values in [nT] with $2.59 \cdot 10^{18}$. See Fig. 5 and Table 11 in subsect. 4.2.3 for detailed information about the secular changes of the dipole coefficients and the geomagnetic pole positions derived therefrom.

Table 4. Dipole and quadrupole spherical harmonic coefficients of the earth's planetary field for the years 1835···1980. They are listed for Schmidt's quasi-normalized spherical functions, eq. (11). Coefficients for epochs 1835., 1885., 1922. are quoted from [fan59, vol. 3, table 10.2]. L denotes the number of grid point values from which the spherical harmonic coefficients have been determined by a least-squares analysis, N the maximum degree and order of the series expansion. Equivolumetric earth's radius $R_E = 6371$ km (MAGSAT: $R_E = 6371.2$ km).

Code refers to the field components used in the analysis. It includes combined analyses of, respectively, all three components (XYZ), the horizontal components (XY), or the vertical component (Z) only, as well as separate analyses of, respectively, all three components (X, Y, Z), or the horizontal components and the vertical component (XY, Z). Accuracy of the coefficients can be estimated from the discrepancy for different analyses.

Author	Epoch	L	N	Code	g_1^0	g_1^1	h_1^1	g_2^0	g_2^1	g_2^2	h_2^1	h_2^2
					10 nT							
Gauss	1835.	84	4	XYZ	−3235	−311	625	51	292	−2	12	157
A. Schmidt	1885.	1800	6 [1]	X, Y, Z [2]	−3192	−212	598	−52	275	62	−71	150
Dyson-	1922.	612	6	XY	−3095	−226	592	−89	299	144	−124	84
Furner				Z [3]	−3046	−232	566	−30	303	132	−87	79
Vestine	1945.	612	6	XY	−3057	−210	581	−127	296	163	−166	54
[Ves47]				Z	−3057	−228	579	−119	294	165	−171	47
Leaton	1965.	540	8	XY	−3037.5	−208.7	576.9	−164.8	295.4	157.9	−199.5	11.6
[Lea65]				Z	−3036.5	−207.0	581.6	−159.5	293.4	159.3	−198.7	8.4
MAGSAT	1979.85	15206 [4]	13	XY, Z	−2998.96	−195.86	560.81 [2]					
[Lan80]	Nov. 6/7			XYZ				−199.48	302.72	166.16	−212.73	−19.61

[1]) Maximum order m = 4.
[2]) Internal coefficients γ_n^m, σ_n^m.
[3]) Up to latitude 60° only.
[4]) Including 5146 satellite observations.

4.1.2.3 Multipole spectra 1835 to 1980

A comprehensive measure of the contribution of terms with the same degree n to the total field potential is the degree variance

$$\sigma_n^2 = (g_n^0)^2 + \sum_{m=1}^{n} \{(g_n^m)^2 + (h_n^m)^2\}. \tag{9}$$

See subsect. 4.1.3.5 for its relation to the mean square flux density $\overline{B^2}$ on spherical surfaces.

Let r be the radius of a sphere which encloses the source region of the earth's field. Then from eq. (19)

$$\overline{B_n^2}(r) = (n+1)\left(\frac{R_E}{r}\right)^{2n+4} \sigma_n^2 = \overline{B_n^2}(R_E) \cdot q^{-(2n+4)} \tag{10}$$

defines the contribution of the n^{th} multipole to the square total flux density averaged over the sphere of radius r, $q = r/R_E$. Plots of σ_n^2 or $\overline{B_n^2}$ versus n in Figs. (21) and (22) are referred to as "spectrum" of the earth's magnetic field.

Table 5 lists the root-mean-square (rms) amplitude $\overline{B_n^2}^{1/2}$ for multipoles from $n=1$ (dipole) to $n=8$. As in Table 4 results from selected analyses for the years 1835···1980 are used, and rms amplitudes are quoted for, respectively, the earth's surface and the surface of the core. To convert the listed values into mean energy densities of the field in units of [J/m^3], divide the square of the tabulated values in [1000 nT] by $8\pi \cdot 10^5$. For the 1965 dipole, for instance, the mean energy densities are, respectively, 0.77 mJ/m^3 at $r = R_E$, and 29.2 mJ/m^3 at $r = 0.545\ R_E$.

Table 5 and the spectra of the earth's planetary field show a remaining dominance of the dipole field. Projected downward to the earth's core, the rms amplitude of the dipole field is still more than twice the rms amplitude of the next largest multipole. Note that all multipole fields for $n \geqq 2$ contribute about equally strongly to the mean flux density at $r = 0.545\ R_E$, which identifies the core's outermost layer as probable source region for the non-dipole part of the planetary field. Any attempt to extrapolate this part downward to greater depth would result in a diverging series of spherical harmonics. Deeper seated sources may exist, but they must produce exclusively toroidal magnetic fields, which would be confined to the core, or deeper seated poloidal sources are varying with time on such a time scale that they are shielded by induction in the highly conducting core itself. No inferences are possible about the source region of the dipole field, which may or may not be identical with that of the non-dipole field.

Table 5 also reveals that the field from terms higher than the quadrupole terms changes smoothly with time. Exceptions may be explained by inaccurate determinations in older analyses. For the dipole rms amplitude a slightly irregular decrease will be noted. The mean rate of change is -24 nT/a which amounts to an annual decrease of 0.055 % for the present dipole. It appears as if this decrease in dipole energy is compensated by a concurrent increase of the quadrupole ($n=2$) and octupole ($n=3$) energy (Fig. 22).

If the dipole and quadrupole rms amplitudes continue to change at their present rates, then about 900 years from now the dipole rms amplitude would have decreased to that of the quadrupole field. Paleomagnetic and also archeomagnetic studies show convincingly, however, that the earth must have had a dominating dipole term for most of its history. Hence, the presently observed rates of change are unlikely to persist for many centuries.

In the first columns of Table 5 a distinction is made between the axial and the non-axial dipole with respect to the earth's axis of rotation. Projected downward to the earth's core the rms amplitude of the non-axial dipole is comparable to the amplitudes of the higher multipoles $n>1$ and thus almost fits into the white spectrum of the non-dipole field.

This supports paleomagnetic evidence that throughout the earth's history the mean dipole field was axial with coinciding geomagnetic and geographic poles. On the other hand, observe that the non-axial dipole presently decreases in such a way that the geomagnetic pole position remains almost unchanged, leaving an angle of 11 degrees between the dipole axis and the axis of rotation. This speaks for a common origin of all dipole terms. See Table 11 in subsect. 4.2.3 for details.

While the orientation of the earth's dipole axis and also the dipole moment appear to be basically the same, past and present, the polarity of the dipole must have changed irregularly from time to time. See subsect. 4.3.3 for the resulting sequence of epochs with normal (as today) and reversed polarity from paleomagnetic studies.

Table 5. Multipole rms amplitudes $\sqrt{\overline{B_n^2}}$ of the earth's planetary field for the years 1835···1980 and two different radii, eq. (10). See Table 4 for data base. $R_E = 6371$ km (epoch 1979.85: $R_E = 6371.2$ km). In the case of the magnetic dipole, rms amplitudes are listed separately for the axial, the non-axial, and the total dipole (n=1) field.

Epoch	Axial dipole	Non-axial dipole	$\sqrt{\overline{B_n^2(r)}}$ [1000 nT]							
			n=1	2	3	4	5	6	7	8
			$r = R_E$ (earth's surface)							
1835	45.75	9.88	46.80	5.82	4.45	3.41				
1885	45.14	8.97	46.02	5.75	4.43	2.73	1.64	0.46		
1922	43.77	8.96	44.68	6.50	4.79	3.11	1.08	0.75		
1945	43.23	8.74	44.11	6.94	5.23	3.27	1.19	0.93		
1965	42.96	8.68	43.82	7.33	5.72	3.29	1.36	0.80	0.36	0.17
1979.85	42.43	8.40	43.26	7.88	5.90	3.20	1.43	0.72	0.34	0.14
			$r = 0.545 \cdot R_E$ (core surface)							
1835	282.9	61.0	289.4	66.1	93	131				
1885	278.1	55.4	284.6	65.2	92	105	(115	59)		
1922	270.7	55.4	276.3	73.7	100	119	76	97		
1945	267.3	54.0	272.7	78.8	109	125	83	120		
1965	265.7	53.7	271.0	83.2	119	126	95	103	84	74
1979.85	262.4	52.1	267.5	89.4	123	122	101	93	81	60

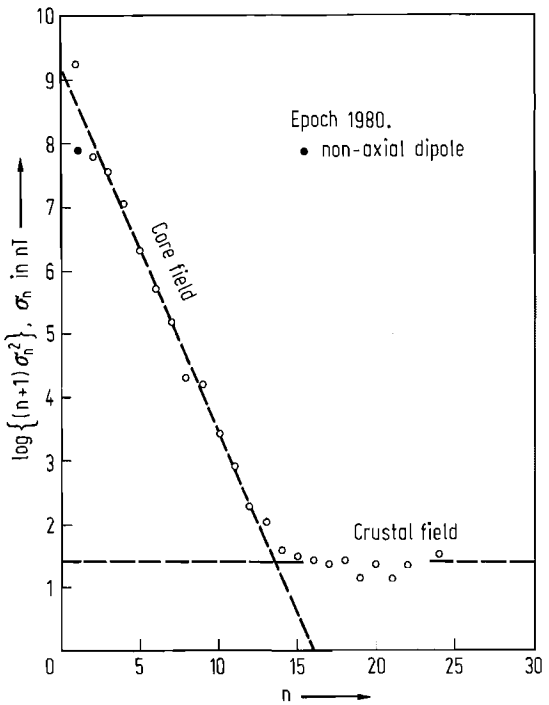

Fig. 22. Secular variations of the earth's planetary field since the year 1835, expressed by the time change of the multipole rms amplitude $\sqrt{\overline{B_n^2}}$ for n=1 (dipole)···8. See legend of Table 5 for further explanations and sources. For $n \leqq 3$ very smooth changes are observed, downward for the dipole, and upward for the quadrupole and octupole. For higher degrees, consistent changes develop since the 1922 analysis with a downward trend of all multipoles except n=5.

Fig. 21. The degree variance spectrum of the earth's magnetic field 1980 for degrees n=1 (dipole)···24 of spherical harmonic functions. See legend of Table 6 for further explanations and sources. Nearly linear changes of the spectrum in logarithmic scale are fitted with two straight lines. Their cross-over lies between n=12 and n=14, separating the spectrum of crustal origin ($n \geqq 14$, sources at zero depth) from the spectrum arising presumably from sources within the earth's core ($n \leqq 12$, sources at 2900 km depth). The dipole value $2 \cdot \sigma_1^2$ lies clearly above the regression line of the core field, which indicates a separate origin for the dipole, while the value for the non-axial dipole component is smaller than expected if it were part of the remaining core field for $n \geqq 2$.

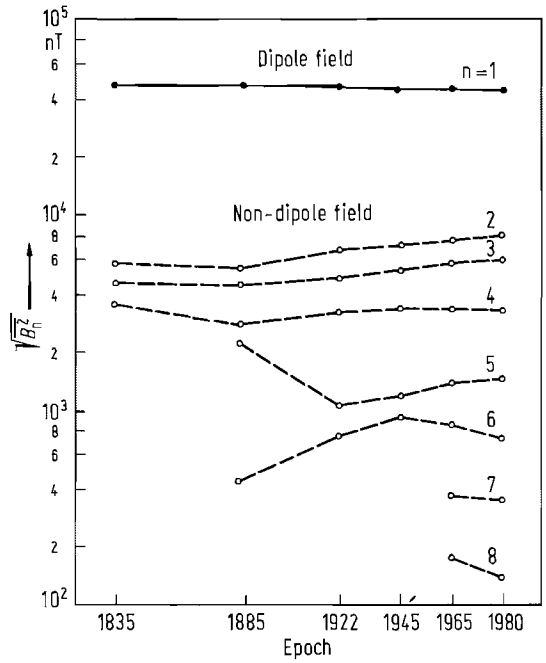

Table 6. Degree variance spectrum of the earth's magnetic field, epoch 1980, See eq. (9) for definition of σ_n^2. The data base for the spherical harmonic analysis are 26500 MAGSAT satellite total intensity and vector field determinations on 14 quiet days between Nov. 5, 1979, and March 15, 1980. Multiply the listed values with $(n+1)^2/(2n+1)$ to obtain, for the n-th multipole, the mean squared intensity of the vertical component, with $n(n+1)/(2n+1)$ to obtain the mean squared intensity of the horizontal components, and with $(n+1)$ to obtain the mean squared total intensity. Adapted from [Lan80, table 2].

n	σ_n^2 nT^2	n	σ_n^2 nT^2	n	σ_n^2 nT^2
1	$934.5 \cdot 10^6$	9	1509.00(9)	17	1.23(6)
2	$20.493 \cdot 10^6$	10	292.30(10)	18	1.30(8)
3	$8.905 \cdot 10^6$	11	67.14(10)	19	0.71(4)
4	$2.066 \cdot 10^6$	12	15.19(9)	20	1.08(7)
5	$338.7 \cdot 10^3$	13	7.49(8)	21	0.63(6)
6	$73.057 \cdot 10^3$	14	2.49(9)	22	0.99(5)
7	$18.20 \cdot 10^3$	15	1.97(8)	23	1.35(9)
8	$2.20 \cdot 10^3$	16	1.63(7)		

4.1.2.4 Spectral separation of core and crustal multipoles

The greatly improved data base by satellite observations allows the determinations of spherical harmonic coefficients of maximum degree $N=12$ and higher, beginning with epoch 1975. Even though the statistical significance of coefficients for such high degrees remains to be verified, a sharp break in the geomagnetic spectrum between $n=12$ and $n=14$ is beyond doubt, [Lan80; Mey83]; and Fig. 21. It is taken to separate the low degree terms of the earth's planetary field from the high-degree terms arising from the earth's magnetized crust. A test of this proposition could come from the secular change of the crustal terms, which should show the relative rate of change of the dipole field when the magnetization is mainly inductive.

From degree $n=2$ to $n=12$ the decrease in rms amplitude for $r=R_E$ with increasing n is well represented by the power law $\overline{B_n^2}=A \cdot b^n$. From a least-squares regression $A=0.1349 \cdot 10^{10}$ (nT)^2, $b=0.27$ [Lan80, eq. 4]. Then, from eq. (10), the radius r for which $\overline{B_n^2}(r)$ equals $\overline{B_{n+1}^2}(r)$ follows as $r=\sqrt{b}\,R_E=3310$ km independent of n, and $\overline{B_n^2}(r)=A/b^2=1.85 \cdot 10^{10}$ (nT)^2. Thus the source region of the core field appears to be bounded by a sphere slightly below the mantle-core boundary at $r=3470$ km.

From $n=14$ to $n=23$ an almost constant rms amplitude of 5.0 nT is observed, putting additional source at zero depth provided that the constant rms amplitude is above the error level of determinations. These shallow sources can be explained by crustal rocks of variable magnetization in the following sense: A crust of uniform thickness with a purely inductive magnetization and a solely depth-dependent susceptibility has no observable surface field [Run75]. Hence, the crustal field comes either from rocks carrying remanent magnetization or from lateral changes in susceptibility. See sect. 4.2 for details on anomalies associated with the crustal field.

It is suggestive to continue the white spectrum of the crustal field at constant level toward $n=1$ and the decreasing spectrum of the core field with the quoted power law beyond $n=12$. If this extrapolation is correct, the non-dipole core field projected downward to the core surface is a random variable with an rms amplitude of presently $1.36 \cdot 10^5$ nT. Note that its secular change must posses a non-random component as exemplified by the "westdrift" of the non-dipole field (cf. subsect. 4.2.3.4).

Similarly, the crustal field appears as a random variable with an rms amplitude of 5.0 nT. Without specific models it is not possible to reproduce the core field at its source level in all small-scale details nor it is possible to identify global trends of the crustal field described by its "hidden" low-degree harmonics. Model calculations for a realistic crust of variable thickness and susceptibility produce comparable rms amplitudes for all degrees, starting with $n=1$ [Mey83].

4.1.3 Spherical harmonics in geomagnetism

4.1.3.1 Series of spherical harmonic functions

Spherical harmonic functions express potential functions $f(\theta, \lambda)$ on a sphere of radius r by series of orthogonal functions of colatitude θ and longitude λ. In geomagnetism geocentric coordinates are used with $\phi=90°-\theta$ and λ as geographic (or geomagnetic) latitude and longitude, respectively. See subsect. 4.2.3.1.2 for the definition of geomagnetic coordinates. Potential (or harmonic) functions satisfy the Laplace equation $\nabla^2 f=0$.

The function $f(\theta, \lambda)$ may be the magnetic potential V or any one of the components of the field vector $\boldsymbol{B} = -\operatorname{grad} V$. In general, internal and external sources with regard to the chosen sphere contribute to the field. Eq. (3) in subsect. 4.2.3.1.2 gives the complete list of coefficients which appear in the series for the internal and external parts of the potential.

The series which express the observed field on the earth's surface, $r = R_E$, are as follows:

$$\begin{aligned} V &= R_E \sum_{n=1}^{N} Y_n, \quad \text{with} \quad Y_n = \sum_{m=0}^{n} \{g_n^m \cos m\lambda + h_n^m \sin m\lambda\} P_n^m(\cos\theta) \\ B_\theta &= -\sum_n \partial Y_n/\partial\theta, \quad \sin\theta B_\lambda = -\sum_n \partial Y_n/\partial\lambda \\ B_r &= \sum_n (n+1) Y_n^*, \quad \text{with} \quad Y_n^* = \sum_m \{a_n^m \cos m\lambda + b_n^m \sin m\lambda\} P_n^m(\cos\theta); \end{aligned} \tag{11}$$

Y_n is a general spherical surface harmonic function of degree n, P_n^m an associated Legendre function of degree n and order $m \leqq n$.

In geomagnetism, by convention, quasi-normalized spherical functions introduced by A. Schmidt are used. The relation of orthogonality for quasi-normalized associated functions is

$$\int_0^\pi P_n^m(\cos\theta) P_{n'}^m(\cos\theta) \sin\theta \, d\theta = \begin{cases} \dfrac{4}{2n+1}, & n = n' \\ 0, & n \neq n' \end{cases} \tag{12}$$

$(m = 0, 1, 2, \ldots)$. Relations which express them for $m = 1, 2, \ldots$ by trigonometric functions can be found in subsect. 4.1.1.6.1, eq. (7). Multiply associated Legendre functions with

$$\sqrt{2(n-m)!/(n+m)!}$$

to obtain for $m = 1, 2, \ldots$ quasi-normalized associated functions. For $m = 0$ quasi-normalized associated functions are identical with zonal spherical harmonics or Legendre polynomials $P_n(\cos\theta)$ of degree n;

$$\begin{aligned} P_0 &= 1 \\ P_1 &= \cos\theta \\ P_2 &= \tfrac{3}{2}\cos^2\theta - \tfrac{1}{2} \\ P_3 &= \tfrac{5}{2}\cos^3\theta - \tfrac{3}{2}\cos\theta. \end{aligned}$$

The series in eq. (11) introduce two sets of coefficients:

(i) Gauss coefficients g_n^m and h_n^m for the potential and the tangential field components,

(ii) the coefficients a_n^m and b_n^m for the radial field component B_r. See eq. (6) in subsect. 4.2.3.1.2 for their relations to the coefficients of the internal and external parts of the observed field.

If this field has only internal or external sources,

$$\begin{aligned} a_n^m &= g_n^m, & b_n^m &= h_n^m & &\text{(internal sources)} \\ (n+1)\, a_n^m &= -n\, g_n^m, & (n+1)\, b_n^m &= -n\, h_n^m & &\text{(external sources).} \end{aligned} \tag{13}$$

In either case, the analysis of B_ϕ (or B_λ) and B_r will be redundant. If the field has internal and external sources, the analysis of B_ϕ (or B_λ) and B_r allows a separation of internal and external parts (cf. eq. (6) in subsects. 4.2.3.1.2 and 4.1.1.3). Because $\boldsymbol{B}$ is irrotational, the relation $\partial(B_\lambda \sin\theta)/\partial\theta = \partial B_\theta/\partial\lambda$ connects B_θ with B_λ which makes the analysis of both tangential components redundant in any case.

4.1.3.2 Spherical harmonic analysis

Because spherical harmonic functions are orthogonal, their coefficients can be found from an observed function $f(\theta, \lambda)$ without dependance on the chosen maximum degree N, in the case of V from

$$\begin{Bmatrix} g_n^m \\ h_n^m \end{Bmatrix} = \frac{2n+1}{4\pi} \int_0^{2\pi} \int_0^{\pi} V \begin{Bmatrix} \cos m\lambda \\ \sin m\lambda \end{Bmatrix} P_n^m(\cos\theta) \sin\theta \, d\theta \, d\lambda. \tag{14}$$

In practice, the coefficients are derived from empirical field values at discrete points and a least-squares solution of eq. (11):

Let the points of observation be equally spaced on J meridians $\lambda_1, \lambda_2, \ldots, \lambda_J$ and I circles of colatitude $\theta_1, \theta_2, \ldots, \theta_I$. Let f_{ij} denote a field value at longitude λ_j and colatitude θ_i. Change now in eq. (11) the order of summations and obtain two sets of linear equations:

1. $f_{ij} = \sum_{m=0}^{N} [\cos m\lambda_j A_{im} + \sin m\lambda_j B_{im}]$

2. $A_{im} = \sum_{n=m}^{N} (n+1) P_n^m(\cos\theta_i) a_n^m$

$B_{im} = \sum_{n=m}^{N} (n+1) P_n^m(\cos\theta_i) b_n^m$

The second set of equations applies to the analysis of B_r. Substitute

$$(n+1) P_n^m a_n^m \quad \text{by} \quad -d P_n^m/d\theta\, g_n^m \quad \text{and} \quad -m P_n^m h_n^m$$

for the analysis of B_ϑ and $B_\lambda \sin\theta$, respectively, with corresponding substitutions for $(n+1) P_n^m b_n^m$.

The least-squares solution of the first set of equations is a harmonic analysis along circles of latitude and yields Fourier coefficients A_{im}, B_{im} which are independent of N. The least-squares solution of the second set of equations, however, depends on N and introduces a truncation error.

If the points of observation are randomly distributed, a single set of equations is solved. This applies in particular when, in the analysis of the earth's planetary field, satellite observations at varying altitudes are included.

4.1.3.3 Spherical harmonic synthesis

The evaluation of eq. (11) with sets of empirical coefficients g_n^m, h_n^m and a_n^m, b_n^m produces synthetic field values for given coordinates (θ, λ) on a sphere of radius $R_E = 6371$ km. If the field has internal and external sources, use eq. (6) in subsect. 4.2.3.1.2 to obtain the required coefficients, otherwise eq. (13). If the field is to be found on a different sphere of radius r, multiply the spherical surface harmonics Y_n and Y_n^* with

$$\left(\frac{r}{R_E}\right)^{n-1} \quad \text{(external sources)}$$
$$\left(\frac{R_E}{r}\right)^{n+2} \quad \text{(internal sources).} \qquad (15)$$

In the analysis with surface observations the earth is taken to be spherical and the same should be done when calculating synthetic field values.

In recent analyses of the earth's planetary field (epoch 1979.85, Table 4, and epoch 1980., Table 11, in subsect. 4.2.3), involving data from satellites, the quoted coefficients refer to the field on an exact sphere of radius $R_E = 6371.2$ km. Thus, multiply Y_n and Y_n^* with

$$\left(\frac{1}{1+\varepsilon(\theta)}\right)^{n+2} \approx 1-(n+2)\,\varepsilon(\theta)$$

to account for the ellipticity of the earth's figure. Here $\varepsilon = f(\frac{1}{3} - \cos^2\theta)$ denotes, in units of R_E, the height of the earth's ellipsoid (flattening $f = 1/298.25$) above the equivolumetric spherical earth at the chosen colatitude.

4.1.3.4 Current function for equivalent current system

The external and internal sources of an observed surface field with the potential $V = R_E \sum_n Y_n$ at $r = R_E$ can be visualized by equivalent currents. They are assumed to flow in a thin spherical shell of a chosen radius R and reproduce exactly the observed field.

Let j be their current density in units of [A/m], derived from a scalar current function ψ:
$j = \mathrm{rot}(\hat{r}\psi) = -\hat{r} \times \mathrm{grad}\,\psi$ with $\hat{r}$ as unit vector in r-direction.

Let ψ be expressed by series of spherical harmonics:

$$\psi = \sum_{n=1}^{N} \psi_n, \quad \text{with} \quad \psi_n = \sum_{m=0}^{n} \{k_n^m \cos m\lambda + l_n^m \sin m\lambda\}\, P_n^m(\cos\theta).$$

Then the requirement that the magnetic field of the currents derived from ψ has at $r=R_E$ the potential V connects the spherical harmonics of V and ψ as follows:

$$\begin{aligned}\psi_n^{(e)} &= -\frac{R_E}{\mu_0}\frac{2n+1}{n+1}\left(\frac{R}{R_E}\right)^n Y_n^{(e)} \quad \text{(external sources, } R>R_E\text{)}\\ \psi_n^{(i)} &= \frac{R_E}{\mu_0}\frac{2n+1}{n}\left(\frac{R_E}{R}\right)^{n+1} Y_n^{(i)} \quad \text{(internal sources, } R<R_E\text{)}.\end{aligned} \tag{16}$$

4.1.3.5 Mean square amplitude and energy density of multipole fields

The expansion into series of spherical harmonic functions allows a simple calculation of the mean square field amplitude $\overline{B^2}$ on any spherical surface and thereby of the mean field energy $\overline{B^2}/2\mu_0$: Let $\boldsymbol{B}_n$ denote the flux density of the field which has the potential $R_E Y_n$ on the surface $r=R_E$; i.e. $\boldsymbol{B}_n$ is the combined field of all multipoles of degree n. Let $\overline{B_{nr}^2}$ be the square radial component, averaged over the surface $r=R_E$. Then from eqs. (11···13),

$$\overline{B_{nr}^2}(R_E)=\begin{cases}\dfrac{(n+1)^2}{2n+1}\sigma_n^2 & \text{(internal sources)}\\[2ex] \dfrac{n^2}{2n+1}\sigma_n^2 & \text{(external sources)}\end{cases} \tag{17}$$

where σ_n^2 is the degree variance as defined in eq. (9). See [Kau67] for its statistical implications for random variables on a sphere. If these averages are taken on spheres of radius r, replace σ_n by $\sigma_n(R_E/r)^{n+2}$ for internal sources and by $\sigma_n(r/R_E)^{n-1}$ for external sources according to the power laws for the field of multipoles (cf. eq. (3) in subsect. 4.2.3.1.2). Adding the mean square of the tangential components,

$$\overline{B_{n\theta}^2}+\overline{B_{n\lambda}^2}=\frac{n(n+1)}{2n+1}\sigma_n^2 \tag{18}$$

for external or internal sources [fan59 III] gives

$$\overline{B_n^2}(r)=\begin{cases}(n+1)\left(\dfrac{R_E}{r}\right)^{2n+4}\sigma_n^2 & \text{(internal sources)}\\[2ex] n\left(\dfrac{r}{R_E}\right)^{2n-2}\sigma_n^2 & \text{(external sources)}.\end{cases} \tag{19}$$

To find the mean energy density of the field in a thin spherical shell of radius r (unit: J/m^3), divide $\overline{B_n^2}(r)$ by $2\mu_0$.

4.1.4 References for 4.1

4.1.4.1 Monographies

aka72 Akasofu, S.-I.; Chapman, S.: Solar-terrestrial physics. Oxford: Clarendon Press **1972**.

aka77 Akasofu, S.-I.: Physics of magnetospheric substorms. Dordrecht-Boston: Reidel Publ. Co. **1977**.

cha40 Chapman, S.; Bartels, J.: Geomagnetism. Vol. 1: Geomagnetic and related phenomena, Vol. 2: Analysis of the data, and physical theories. Oxford: Oxford University Press **1940** (reprinted 1951, 1962).

fan59 Fanselau, G. (ed.): Geomagnetismus und Aeronomie. Band 1/1: Theorie der elektromagnetischen Felder (P. Mauersberger), Band 1/3: Elektrische und magnetische Eigenschaften der festen Körper (F. Frölich), Band 1/E: Kugelfunktionen (H. Kautzleben), Band 2: Geomagnetische Instrumente und Meßmethoden (H. Wiese, H. Schmidt, O. Lucke, F. Frölich), Band 3: Über das aus dem Erdinnern stammende Magnetfeld (P. Mauersberger, O. Lucke, R. Lauterbach, F. Frölich). Berlin: VEB Deutscher Verlag der Wissenschaften **1959–1965**.

joh61 Johnson, F.S. (ed.): Satellite environment handbook. Stanford/Calif.: Stanford University Press **1961**.

mat67 Matsushita, S.; Campbell, W.H. (eds.): Physics of geomagnetic phenomena (2 vols.). New York-London: Academic Press **1967**.

may80 Mayaud, P.N.: Derivation, meaning, and use of geomagnetic indices. Geophysical monography 22. Washington D.C.: American Geophysical Union **1980**.

nis78 Nishida, A.: Geomagnetic diagnosis of the magnetosphere. Physics and chemistry in space, vol. 9. New York-Heidelberg-Berlin: Springer **1978**.

par83 Parkinson, W.D.: Introduction to geomagnetism. Edinburgh-London: Scottish Academic Press **1983**.

run82 Runcorn, S.K.; Creer, K.M.; Jacobs, J.A. (eds.): The earth's core: Its structure, evolution and magnetic field. London: The Royal Society **1982**.

4.1.4.2 Special references

Bab80 Babour, K., Mosnier, J.: Geophys. J. **60** (1980) 327.

Far68 Fairfield, D.H.: J. Geophys. Res. **73** (1968) 7329.

Fil67 Filloux, J.H.: Oceanic electric currents, geomagnetic variations and the deep electrical conductivity structure of the ocean-continent transition of central California. Ph.D. Thesis, Univ. Calif. San Diego **1967**.

For61 Forbush, S.E., Casaverde, M.: Equatorial electrojet in Peru. Carnegie Institution of Washington Publication **620** (1961).

For67 Forbush, S.E., Beach, L.: Carnegie Institution of Washington, Year Book **65** (1967) 28.

Gla84 Glaßmeier, K.H., Lester, M., Mier-Jedrzejowicz, W.A.C., Green, C.A., Rostoker, G., Orr, D., Wedeken, U., Junginger, H., Amata, E.: J. Geophys. **55** (1984) 108.

Har63 Hartmann, O.: Behandlung lokaler erdmagnetischer Felder als Randwertaufgabe der Potentialtheorie. Abh. Akad. Wiss. Göttingen, Math.-Phys. Klasse, Beiträge zum Internationalen Geophys. Jahr **9** (1963).

Kau67 Kaula, W.M.: Rev. Geophys. **5** (1967) 83.

Lan80 Langel, R.A., Estes, R.H., Mead, G.D., Fabiano, E.B., Lancaster, E.R.: Geophys. Res. Letters **7** (1980) 793.

Lan82 Langel, R.A., Estes, R.H.: Geophys. Res. Letters **9** (1982) 250.

Lea65 Leaton, B.R., Malin, S.R.C., Evans, M.J.: J. Geomagn. Geoelectr. **17** (1965) 187.

Mal73 Malin, S.R.C.: Worldwide distribution of geomagnetic tides. Phil. Trans. R. Soc. London **A274** (1973) 551.

McD67 McDonald, K.L., Gunst, R.H.: An analysis of the earth's magnetic field from 1835 to 1965. Institutes for Environmental Research (ESSA, Boulder/Colorado) Techn. Report 46-IES1, **1967**.

Mey83 Meyer, J., Hufen, J.-H., Siebert, M., Hahn, A.: J. Geophys. **52** (1983) 71.

Nis68 Nishida, A.: J. Geophys. Res. **73** (1968) 1795.

Par77 Parkinson, W.D.: An analysis of the geomagnetic diurnal variation during the International Geophysical Year. Bureau of Mineral Resources, Geology and Geophysics (Dept. National Resources, Canberra/Australia), Bulletin **173** (1977).

Pri63 Price, A.T., Wilkins, G.A.: Phil. Trans. R. Soc. London **A256** (1963) 31.

Ros75 Rosenbauer, H., Grünwaldt, H., Montgomery, M.D., Paschmann, G., Sckopke, N.: J. Geophys. Res. **80** (1975) 2723.

Run75 Runcorn, S.K.: Nature **253** (1975) 701.

Sie71 Siebert, M.: Maßzahlen der erdmagnetischen Aktivität, in: Flügge, S. (ed.), Handbuch der Physik Band XLIX/3 (1971) 206.

Sug60 Sugiura, M., Chapman, S.: The average morphology of geomagnetic storms with sudden commencement. Abh. Akad. Wiss. Göttingen. Sonderheft **4** (1960).

Sug65 Sugiura, M., Heppner, J.P.: The earth's magnetic field, in: W.N. Hess (ed.), Introduction to Space Science, New York-London-Paris: Gordon and Breach **1965**.

Win81 Winch, D.E.: Phil. Trans. R. Soc. London **A303** (1981) 1.

4.1.4.3 Tabular works

The earth's planetary field

Annual values of geomagnetic elements since 1941 (compiled under the general supervision of B.R. Leaton). Royal Observatory Bulletins No. 134, London, Her Majesty's Stationery Office **1967**.

Bar78 Barraclough, D.R.: Spherical harmonic models of the geomagnetic field. Geomagnetic Bulletin 8 Institute of Geological Sciences, London: Her Majesty's Stationery Office **1978**.

Boc48 Bock, R., Schumann, W.: Katalog der Jahresmittel der magnetischen Elemente der Observatorien und der Stationen, an denen eine Zeitlang erdmagnetische Beobachtungen stattfanden. Abh. Geophys. Institut Potsdam Nr. 8-11, Berlin: Akademie-Verlag **1948**.

Lea71 Leaton, B.R., Barraclough, D.R.: Grid values of the International Geomagnetic References Field 1965. Paris (V), IUGG Publ. Office (39 Ter, Rue Gay-Lussac) **1971**.

Ves47a Vestine, E.H., Laporte, L., Lange, I., Cooper, C., Hendrix, W.C.: Description of the earth's main field and its secular change, 1905-1945. Carnegie Institution of Washington Publication 578, Washington D.C. **1947**.

Ves47b Vestine, E.H., Laporte, L., Lange, I., Scott, W.E.: The geomagnetic field, its description and analysis. Carnegie Institution of Washington Publication 580, Washington D.C. **1947**.

Geomagnetic variations and indices

Gup68 Gupta, J.C., Chapman, S.: Manual of the coefficients of the first four harmonics of the solar and lunar daily geomagnetic variations computed from IGY/C and certain other data. Manuscript 68-110. National Center Atmospheric Research, Boulder/Colorado, **1968**.

Pri68 Price, A.T., Stone, D.J.: The quiet-day magnetic variations during the IGY. Vol. 35, pp. 64-269. Annals International Geophysical Year, Oxford Pergamon Press **1964**.

Ves47b See under "The earth's planetary field".

Bar62 Bartels, J.: Collection of geomagnetic planetary indices Kp and derived indices, Ap and Cp for the years 1932 to 1961. IAGA Bulletin No. 18, Amsterdam, North-Holland Publ. Co. **1962**.

May73 Mayaud, P.N.: A hundred year series of geomagnetic data 1868-1967; indices aa, storm sudden commencements. IAGA Bulletin No. 33. Paris (V), IUGG Publ. Office (39 Ter, Rue Gay-Lussac) **1973**.

May77 Mayaud, P.N., Romana, A.: Supplementary geomagnetic data 1957-1975. Paris (V), IUGG Publ. Office (39 Ter, Rue Gay-Lussac) **1977**.

Geomagnetic indices K and C (1940-1969); Geomagnetic data: Indices K and C, rapid variations (1957-69). IAGA Bulletin No. 12, 12a-12x, Amsterdam, North-Holland Publ. Co. 1948-63; Paris (V), IUGG Publ. Office (39 Ter, Rue Gay-Lussac) **1964-69**.

Geomagnetic data: Indices, rapid variations, magnetic storms (1970-79). IAGA Bulletin No. 32a-32j. Paris (V), IUGG Publ. Office (39 Ter, Rue Gay-Lussac) **1972-1980**.

Data sources

1. Geomagnetic observatory data:

   World Data Center A, National Oceanic and Atmospheric Administration 325 Broadway, Boulder, CO 80303, U.S.A.

   World Data Center B, Molodezhnaya 3, Moscow 117296, USSR.

   World Digital Data Centre C1, Geomagnetism Unit, Institute of Geological Sciences, Murchison House, West Main Road, Edinburgh EH9 3LA, Scotland, U.K.

   World Data Centre C1, Meteorological Institute, 100 Lyngbyvej, 2100 Copenhagen ϕ, Denmark.

   World Data Center C2, WDDC-C2 for Geomagnetism, Indian Institute of Geomagnetism, Colaba, Bombay 5, India.

2. Spherical harmonic coefficients for the earth's magnetic field and magnetic satellite data:

   World Data Center for Rockets and Satellites, Code 601, NASA Goddard Space Flight Center Greenbelt, MD 20771, U.S.A.

3. World charts of the earth's magnetic field (compiled by the US Naval Oceanographic Office and the UK Institute of Geological Sciences):

   Defense Mapping Hydrographic/Topographic Center, Washington D.C. 20315, U.S.A.

4. Geomagnetic Indices (Ap, ap, Cp):

   Institut für Geophysik, Herzberger Landstraße 180, Postfach 2341, D-3400 Göttingen (F.R.G.).